LOCATING THE INNER EDGE OF A NEUTRON STAR CRUST

By

Milton William van Rooy

Thesis presented in partial fulfillment of the requirements for the degree of
MASTER OF SCIENCE
at Stellenbosch University.

Department of Physics
Faculty of Natural Sciences
Supervisor : Doctor S.M. Wyngaardt
Co-supervisor : Professor G.C. Hillhouse
December 2010

DECLARATION

By submitting this thesis electronically, I declare that the entirety of the work contained therein is my own, original work, that I am the owner of the copyright thereof (unless to the extent explicity otherwise stated) and that I have not previously in its entirety or in part submitted it for obtaining any qualification.

Signature

ABSTRACT

The overall goal of this project is to study neutron star properties and locate the transition density from the core to the crust using fifteen parameter sets of the effective Skyrme nucleon-nucleon interaction within a method called the dynamical method. Although another approach used to describe nucleon-nucleon interactions called the modified Gogny interaction is briefly discussed in this work, along with a second method for locating the transition density called the thermodynamical method, results using this interaction and method were not generated, but lays some foundation for a PhD project to be undertaken and potentially showing the relation between the interactions and results. The importance of results depends on how well other theoretical approaches to the problem can reproduce those results and to what accuracy. For models to be valid there also has to be good agreement between the theoretical results and known observables. In this project some properties of neutron stars, such as the equation of state, saturation density, binding energy, symmetry energy, slope and incompressibility parameters of symmetry energy are studied. The transition density is located using the dynamical method. Results of the fifteen Skyrme parameter sets show excellent agreement with the published values of the properties of neutron stars and are consistent with their empirical values inferred from nuclear laboratory data, thus validating the use of the Skyrme interactions for describing nuclear matter.

OPSOMMING

Die hoofdoel van hierdie projek is om neutron ster eienskappe te bestudeer en die oorgangsdigtheid vanaf die kors na die kern te vind deur gebruik te maak van vyftien parameter stelle van die effektiewe Skyrme nukleon-nukleon interaksie binne ‘n metode genaamd die dinamiese metode. Alhoewel ‘n ander benadering vir die beskrywing van nukleon-nukleon interaksies, genaamd die gewysigde Gogny interaksie kortliks in hierdie werk beskryf word, asook ‘n tweede metode, genaamd die termodinamiese metode om die oorgangsdigtheid te bepaal, was resultate vir hierdie interaksie en metode nie gegenereer nie, maar lê die fondasie vir verdere werk aan ‘n PhD projek wat die verband tussen die twee interaksies en resultate kan wys. Die belangrikheid van resultate hang af van hoe goed ander teoretiese benaderinge tot die problem daardie resultate kan herproduseer en tot watter akkuraatheid. Vir modelle om geldig te wees moet daar ook goeie ooreenkomste wees tussen teoretiese resultate en bekende waarneembare eienskappe. In hierdie projek word sommige eieskappe van neutron sterre, soos die toestandandsvergelyking, versadigingsdigtheid, bindingsenergie, simmetrie-energie, gradiënt en onsaampersbaarheids parameters van die simmetrie-energie bestudeer. Die oorgangsdigtheid word dan gevind deur gebruik te maak van die dinamiese metode. Resultate van die vyftien Skyrme interaksie parameter stelle wys goeie ooreenstemming met die gepubliseerde waardes van die eienskappe van neutron sterre en is konsistent met hulle empiriese waardes afgelei van kern laboratorium data, wat die geldigheid van Skyrme interaksies vir die beskrywing van kern-materie bevestig.

ACKNOWLEDGEMENTS

This project would not have been possible without the support of the following people and institutions:

- The South African Square Kilometre Array (SKA) Project which provided financial support.
- The University of Stellenbosch.
- My supervisor Dr. S.M. Wyngaardt and co-supervisor Prof. G.C. Hillhouse.
- My family who always supported me.
- My God who gave me the strength to finish this project and protected my family.

TABLE OF CONTENTS

LIST OF FIGURES

.

LIST OF TABLES

CHAPTER 1
Introduction

The first thing that comes to mind when one hears the word “neutron star”, is a star composed of neutrons. This is not far from the truth, as the bulk of a neutron star consists of a neutron fluid, in equilibrium with about 5% protons and electrons. As such, an over simplified view of a neutron star is a gigantic nucleus, with density similar to that of nuclear matter and an average radius of 10 km and mass of 1.4 solar masses [1, 2]. Whereas nuclei are bound by the isospin-symmetric nuclear force, neutron stars are bound by gravity.

The proposal made by Baade and Zwicky in 1934 that a neutron star might be the end product of the supernova collapse of a normal star, led Oppenheimer and Volkoff in 1939 to analyze the structure of a star consisting of a degenerate neutron gas at high density [1]. They showed that the degeneracy was so complete that the temperature has no effect and the only relationship is between energy density and pressure. For the next 30 years most physicists and astronomers did not take the possibility of neutron stars very seriously (since the stars are so small, people felt that the prospects for observing them were minimal, and thus little effort was expended on theory or observation of neutron stars). This changed dramatically in 1967 when Jocelyn Bell observed a pulsating signal from outer space, with characteristics unlike the scintillation signals from quasars, which she was observing. The origins of the pulsating signals were thought to be man-made or even the first radio signals from an extraterrestrial civilization, but in 1968 Hewish and Bell published their findings in a Nature letter and explained the origin to be a rapidly rotating neutron star, now known as a pulsar [1]. Since then the problem has been to find the relationship between energy density and pressure, described by the equation of state (EOS). Given the EOS, a unique relation between mass and radius can be deduced, so that it is theoretically possible to work back from observed parameters and constrain the EOS itself. The EOS is vital for describing neutron stars and it is a continuous effort to develop and constrain the EOS especially for densities higher than the nuclear saturation density. Neutron stars provide an exciting test bed for the extreme physics of nuclear matter. They are hotter, denser and have stronger magnetic and gravitational fields than anything we can hope to create on earth. Therefore, the neutron star crust and surface constitute an extra-terrestrial laboratory for studying physics under extreme

physical conditions. Neutron stars, as compact objects and one of the possible endpoints of stellar evolution, have a remarkable richness of internal structures, the study of which encompasses a variety of research fields: astrophysics, nuclear physics, particle physics and atomic physics. Because of such richness, neutron stars continue to furnish astonishingly fresh information in these fields.

Our current knowledge of neutron stars is derived from observation of their electromagnetic spectrum. This has given information that, along with the currently accepted laws of physics, has helped create a model for the structure of the star. Still, there are observations that are as yet not explained. It is the responsibility of theorists to try to provide useful models that can be tested against the available data from observations and experiments.

1.1 Birth of a neutron star

For billions of years stars like our sun are in a state of thermal equilibrium. These stars have three possible end states: a white dwarf, a neutron star or a black hole, depending on the mass of the star. These states are reached when a normal star collapses under its own gravity. For a star more massive than about 8 solar masses, a neutron star will form. When the hydrogen fuel in the star’s centre is exhausted, the energy production by hydrogen fusion terminates, causing the star's thermal equilibrium to be disturbed, and the core of the star (now consisting mainly of helium) to contract [3, 4]. The temperature and the pressure in the core rise, until they become high enough for helium fusion to start and the star reaches a new thermal equilibrium. Meanwhile a hydrogen-burning shell has formed around the core, and the outer envelope of the star has expanded to giant dimensions [3]. In turn, the helium in the core becomes exhausted, the process repeats and during subsequent stages, heavier and heavier elements fuse until an iron core is formed [1, 3]. Because iron is the most tightly bound nucleus the star is no longer able to produce energy in the core via further nuclear burning stages. Nuclear reactions will continue, however, because of the extremely high temperatures in the massive star's core. Due to photodissociation at such extreme temperatures the iron nuclei in the core are destroyed. During this process the nuclear binding energy is used up, which causes the pressure to drop [4, 5]. As a result the core starts to cool and contract, the density increases and the free electrons are boosted to higher energy levels. The degenerate electrons become relativistic and eventually the electron

speed, required for electron degeneracy to balance the crushing effect of the core's gravity, becomes greater than the speed of light. As such, electron degeneracy cannot support the core. The electrons are captured by the protons (inverse beta-decay) to form neutrons, which in turn become degenerate [3]. The neutrinos, which escape directly from the core, result in further energy loss and even faster collapse. The core collapses so rapidly that it effectively collapses out from under the stellar envelope (matter surrounding the core). When neutron degeneracy sets in, the collapse is halted, the core will stiffen and the in-falling material from the envelope will rebound in a shockwave outward from the core, releasing an enormous amount of energy, driving the remaining material from the envelope outward, compressing it and heating it in a supernova explosion [1, 3]. The net result is the formation of a neutron star.

1.2 Neutron star structure

According to current views, a neutron star consists of four main regions enclosed by a thin layer of atmosphere [4, 6], as shown in figure 1.1. These four regions are: an outer crust, an inner crust, an outer core and an inner core. The thin atmosphere is made of plasma, consisting of electrons, nuclei and atoms [6, 7]. Its geometrical depth varies from ten centimetres in a hot star to a few millimetres in a colder star.

The solid outer crust extends for a few hundred meters, from the bottom of the atmosphere to a layer of density $4.3 \times 10^{11} g.cm^{-3}$ (neutron drip density ρ_d, when the pressure inside the neutron star becomes so high, that more and more nucleons get squashed together until the nuclear force repels them and neutrons start to leak from the nucleus) and consists of degenerate electrons in beta-equilibrium with ions (heavy nuclei) [2, 4, 6]. The nuclei are arranged in a body-centred cubic (bcc) lattice [7].

The inner crust extends (possibly for several kilometers) from the neutron drip density to the base where nuclei "melt" (do not exist anymore) and a transition to homogeneous nucleonic matter occurs, signalling the start of the outer core [7]. The inner crust contains free electrons, free neutrons and neutron rich atomic nuclei, with the fraction of free neutrons increasing with density [2, 4, 8]. However, specific models of effective nucleon-nucleon (NN) interactions predict that, in the melting process, rodlike and slablike nuclei embedded in a gas of neutrons, as

well as rodlike and roughly spherical neutron-gas regions (bubbles) surrounded by a nucleon liquid, exist in the bottom layer [8, 9, 10, 11]. At a density where roughly spherical nuclei are so closely packed that they occupy about 1/8 of the system volume, the nuclei tend to be elongated and eventually fuse into nuclear rods. The advantage of this rod formation is a reduction in the total surface area from the roughly spherical case. However, whether bubbles and nonspherical nuclei actually appear in neutron star crusts depends on the critical density at which proton clustering (the fraction of free neutrons increases with density, as such the nuclei can be regarded as proton clusters in the neutron gas) instability occurs in uniform nuclear matter [8]. The inner crust may contain a neutron superfluid.

At the crust-core interface the nuclei disappear completely and merge into a uniform mixture of nucleons and leptons [12, 13]. The outer core may be several kilometers deep. More massive stars may also possess an inner core, whose composition is largely unknown. A reliable theory of super dense neutron star matter does not yet exist.

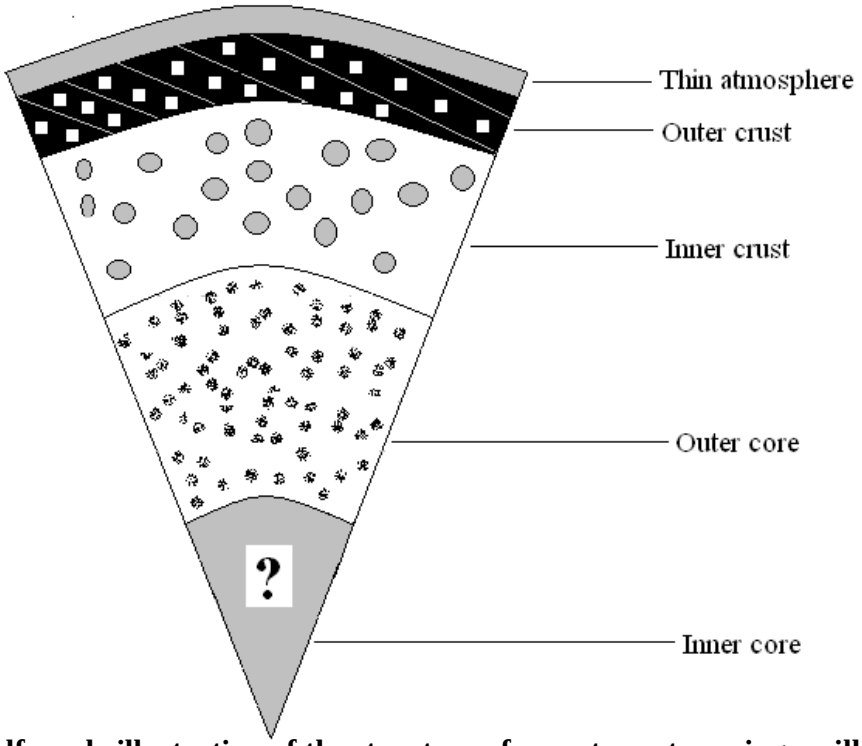

Figure 1.1: A self-made illustration of the structure of a neutron star using an illustration from http://www.astroscu.unam.mx/neutrones/NS-picture/NStar/NStar-I.gif [14] as a reference.

1.3 Neutron star EOS

Different models exist for describing nuclear matter, from the relativistic mean-field approach to the non-relativistic Skyrme interaction [3, 7, 8]. Nuclear matter properties depend critically on the EOS of the chosen model, with each model giving a unique relation between energy density and pressure. The success of the model is rated by how well it can reproduce the experimentally inferred values of nuclear matter properties (defined in section 2.3) such as nuclear symmetry energy, binding energy, saturation density and the incompressibilty coefficient. The EOS is thus the starting point for studying the crust-core transition density. For symmetric nuclear matter ($N = Z$, equal number of neutrons, N and protons, Z), the EOS is relatively well-determined after about more than 30 years of studies in the nuclear physics community. The incompressibility of symmetric nuclear matter at its saturation density (ρ_0) has been determined to be $240\pm20\ MeV$ from the nuclear giant monopole resonances (GMR) [15, 16] and the EOS at densities of $2\rho_0 < \rho < 5\rho_0$ has also been constrained by measurements of collective flows in nucleus-nucleus collisions [17] and of sub-threshold kaon production [18, 19] in relativistic nucleus-nucleus collisions. On the other hand, for asymmetric nuclear matter, the EOS, especially the density dependence of the nuclear symmetry energy, is largely unknown. Although the nuclear symmetry energy at ρ_0 is known to be around 30 MeV from the empirical liquid-drop mass formula [20, 21], its values at other densities are poorly known**.** The symmetry energy is important for understanding the structure of radioactive nuclei, the reaction dynamics induced by rare isotopes, and the liquid-gas phase transition in asymmetric nuclear matter. Many radioactive beam facilities around the world are currently under construction or in planning, such as the Radioactive Ion Beam (RIB) Factory at RIKEN in Japan [22], the FAIR/GSI in Germany [23], SPIRAL2/GANIL in France [24], and the Facility for Rare Isotope Beams (FRIB) in the USA [25]. These facilities aim to extract information on the isospin dependence of in-medium nuclear effective interactions as well as the EOS of isospin asymmetric nuclear matter, particularly its isospin-dependent term or the density dependence of the nuclear symmetry energy. The heavy-ion collisions induced by these neutron-rich radioactive beams are not expected to create the same matter and conditions as in neutron stars, even though the same elementary nuclear interactions are at work in the two cases. Neutron star matter differs from the high density systems produced in heavy ion collisions by two essential features: a) Matter in high energy collisions is still governed by the charge symmetric nuclear force while neutron star matter is

bound by gravity. Since the repulsive Coulomb force is much stronger than the gravitational attraction, neutron star matter is much more asymmetric than normal nuclear matter. b) The second essential difference is caused by the weak interaction time scale of $\sim 10^{-10} s$, which is small in comparison with the lifetime of the star, but large in comparison with the characteristic time scale of heavy ion reactions.

For these reasons normal nuclear matter is subject to the constraints of isospin symmetry and strangeness conservation, but neutron star matter has to obey the constraints of charge neutrality and generalized beta-equilibrium with no strangeness conservation, because strangeness can change by zero or one unit in weak interactions. Extracting the equation of state of dense matter from collisional data and extrapolating it from the hot conditions in the collision volume to the relatively cold temperatures, $\sim 1 - 10\ keV$, in neutron star interiors, would enable one to construct more accurate models of neutron stars.

1.4 Importance of the neutron star crust and significance to the Square Kilometre Array

South Africa and Australia are the two finalists in a bid to host the world's most powerful radio telescope, the Square Kilometre Array (SKA) consisting of approximately 3 000 antennas. The South African Square Kilometre Array Project aims to construct the core of the SKA telescope in the Northern Cape Province of South Africa, with antenna stations in Namibia, Botswana, Mozambique, Madagascar, Kenya and Zambia. The combined collecting area of all the antennas will add up to one square kilometre, from which the SKA gets its name. The result of the bid will be announced in 2012.

The SKA will put South Africa at the forefront of astronomy research, equipped with other major astronomy facilities in the region, such as the South African Large Telescope (SALT) in the Karoo, the High Energy Stereoscopic System (HESS) gamma ray telescope in Namibia and the Karoo Array Telescope (MeerKAT) which is currently being constructed as a precursor instrument for the SKA. These facilities will give scientists opportunities to participate and collaborate in cutting edge research. In particular, relevant to this project, the SKA could be used to observe neutron star properties and collect neutron star data.

An understanding of the crust of a neutron star is important for a number of observable properties of the star. For example, neutrino emission from the crust could play an important role in the thermal evolution of the star if neutrino emission from the core was suppressed by superfluidity. At a critical density inside the neutron star the neutrons, protons and electrons which are many-body fermion systems may undergo a phase change to a so-called superfluid state. In the case of charged particles the state will be superconducting (zero electrical resistance) [4]. Inside a neutron star two neutrons can be bound in the field of other nucleons, held together by the interaction of their nuclear magnetic moments with the surrounding nucleons, forming pairs. A pair of fermions has integer spin and is therefore a boson, thus pairs of neutrons are presumed to have similar behavior to liquid ^{4}He, which forms a superfluid below $T = 2.19\ K$ with essentially zero viscosity. Similarly in neutron stars this behavior may occur whenever the thermal energy kT is less than the latent heat (the heat required or expelled by a system to establish a phase change associated with the phase change to a paired state). It is known from laboratory nuclei at nuclear densities ($2.8 \times 10^{14}\ g\ cm^{-3}$) that both neutrons and protons have undergone a pairing transition in cold nuclear matter and that the latent heat is ~ 1-2 MeV, indicating that superfluidity in neutron stars can be expected [4]. Also in models of glitches (sudden leaps in the rotation period of pulsars) that invoke coupling between the superfluid in the crust of a neutron star and a solid crust, the moments of inertia of the various components of matter in the crust play a crucial role [8]. In determining the crustal properties the inner part of the crust close to the transition to the uniform matter in the core is of utmost importance, because of the large density gradient, it is in this region where most of the crustal matter resides. The density of the transition from the crust to the interior is an essential input into calculations concerning the dynamics of the crust of a neutron star. Observing a rapid change in the EOS with density could signal transition to an exotic phase of matter [26]. Possibilities for new high density phases include pion or kaon condensates, strange quark matter, and/or a colour superconductor. This indicates the need to understand the crust-core transition region well.

This project aims to calculate the density at the phase boundary between the liquid matter of the interior of a neutron star and the solid matter that comprises the crust. Different methods exist to calculate this transition density, as described in chapter 3, sections 3.2 and 3.3. Results of the project will consolidate the knowledge of the crust-core transition region. In order to interpret

observational data from telescopes or experiments, one needs to develop reliable models of matter under extreme conditions. Currently the knowledge base in South Africa pertaining to models that describe the interior of pulsars and neutron stars, from the nuclear perspective, is very limited.

This research forms a fundamental part of a larger project to calculate the moment of inertia of different parts of the neutron star interior. If the transition density from the crust to the core is known, the moment of inertia of the crust can be calculated. There are proposals that glitching in pulsars is due to the transfer of angular momentum between the crust and the core. As shown in Ref. [27] the observed properties of glitches can be related to the theoretical calculated ratio of the moment of inertia of the crust and the liquid interior of the star. This can provide constraints on the equation of state of the neutron star crust and interior. The procedure is described in Ref. [27].

The larger project will combine observational neutron star data with theoretical descriptions of neutron stars and dense matter. This research forms an integral part of this project and therefore will also entail exposure to current neutron star research.

Since these theoretical studies can only be validated through good agreement with observed properties of neutron stars, close co-operation between theorists and astronomers is crucial in the study of neutron stars. The converse is also true: to explain observational results, theoretical modelling is needed to predict certain observed properties. Only through this interplay between theoretical and observational science can the understanding of our universe be advanced.

In chapter 2 the conditions under which the neutron star is studied, are described along with their implications which can be understood through equations. The conditions affect the construction of the EOS from which properties of neutron stars can be derived. These properties are also discussed. The end of chapter 2 looks at the effective nucleon-nucleon interactions used to construct the EOS's. The Skyrme interaction with fifteen of its most popular parameter sets is the main focus of this project, but the modified Gogny interaction is briefly discussed.

Chapter 3 describes two of the methods which can be used to calculate the crust-core transition density. This is done by searching for the density at which the uniform liquid in the core first

becomes unstable against small-amplitude density fluctuations, which defines the transition density as the last stable phase from the inner core. The Skyrme interaction will be used within the dynamical method to calculate the transition density, the second method, the thermodynamical method, is also discussed and compared to the dynamical method.

Results of the properties of neutron stars calculated using the fifteen parameter sets of the Skyrme interaction are given in chapter 4 and compared to the published values. Transition densities are listed for the fifteen parameter sets and compared. Behaviour of the EOS and properties of neutron stars are also discussed.

A brief summary of this work is given in chapter 5 and concluding remarks are made. Appendix A gives a description of the FORTRAN90 code which was used to do the calculations.

CHAPTER 2

Models for describing neutron star matter

2.1 Introduction

Neutron stars are the perfect environment to study nuclear matter under extreme conditions of momentum transfer and densities. The holy grail of nuclear physics would be the development of a universal nuclear theory, meaning that it is well established in its methodology and can be applied across the chart of nuclides. The basic question in all neutron star matter (protons, neutrons and electrons) is to understand what the relationship is between the pressure and energy density, the equation of state (EOS). In this project two interactions, namely Skyrme interactions within the Hartree-Fock approach and the modified Gogny momentum dependent interaction (MDI) are used to describe infinite neutron star matter at zero temperature. In this chapter the conditions under which the transition density will be studied are discussed. Properties of symmetric nuclear matter are defined and EOS's are constructed using the above mentioned interactions. These interactions are then used to calculate the properties of neutron stars and study the crust-core transition density, thereby verifying what others have done in order to gain experience in this field. The EOS's using various Skyrme forces are well known for their simple forms and successful descriptions of many interesting phenomena [28, 29]. A very useful feature of both the MDI and the Skyrme interaction is that analytical expressions for many interesting physical quantities in asymmetric nuclear matter at zero temperature can be obtained. Other nuclear models exist for constructing the EOS. Many-body approaches and the interactions used show similar behaviour in the symmetry energy and binding energy at sub-saturation densities. Moving to higher densities they begin to show different behaviours in the EOS and symmetry energy. In the Relativistic Mean-field (RMF) model [30] and Brueckner-Hartree-Fock model [29] the symmetry energy rises continuously as a function of density. In other models such as the variational many-body approach the symmetry energy shows the expected rising behaviour in the beginning but then starts to fall after saturation density [31]. The different behaviour of the different models at high densities provides motivation for further investigation. In this work the behaviour that the fifteen Skyrme parameter sets show will be investigated to see what causes the different behaviour and how the parameters can be changed to alter the behaviour.

2.2 Equilibrium conditions

After a few years a newly formed neutron star will become cold on the nuclear scale ($\sim 1 \times 10^6 K$). Ideally, it will be in the lowest energy state, and the neutrinos and photons produced by the reactions in achieving the lowest state, will have escaped from the star. After the star has dropped in temperature below an MeV, it can be referred to as cold for the purpose of computing the energy and pressure, but the temperature is still very high compared to the neutrino masses (0.1 eV or greater [32]), so they have velocity sufficient to escape, if not light velocity [3]. In this project a neutron star is studied when it has reached its ground state at each relevant baryon density. The neutron star is assumed to be static, spherical symmetric. Since the Coulomb forces are much stronger than the gravitational forces on the nuclear scale, neutron stars are assumed to be macroscopically charge neutral. A net charge would result in very disruptive Coulomb forces in the neutron star [3]. The temperature of neutron star matter can be taken as zero in a good approximation because it is much lower than the Fermi energies of neutrons and protons.

Free neutrons (n) are unstable and beta-decay into a proton (p), electron (e^-) and anti-neutrino ($\bar{\upsilon}_e$)

$$n \rightarrow p + e^- + \bar{\upsilon}_e.$$

Neutrons have a short half-life of approximately 10 minutes, compared to the lifespan of a neutron star. As such, the beta-decay process will produce a significant number of electrons, some of which will become relativistic at high densities and if all electron energy levels in the Fermi sea are occupied up to the one that the emitted electron would fill, beta-decay is blocked. Thus there is a critical density for the onset of inverse beta-decay (the capture of an electron by a proton to form a neutron and a neutrino (υ_e))

$$p + e^- \rightarrow n + \upsilon_e \, .$$

Beta-decay and inverse beta-decay will continue until an equilibrium state called beta-equilibrium is reached. In beta-equilibrium the system is in its ground state, meaning that at each

baryon density $\rho = \rho_p + \rho_n$, the proton and neutron number densities (ρ_p and ρ_n) are such that the energy density ($\mathcal{E}$) of the system is at a minimum. In terms of chemical potentials μ_q, the beta-equillibrium condition can be expressed as [28]

$$\mu_q = \frac{\partial \mathcal{E}}{\partial \rho_q}, \tag{2.1}$$

where $q \, \epsilon \, \{n, p, e\}$. The chemical potential of neutrons is the minimum energy required to add a neutron to a nucleus at fixed proton number, similarly the chemical potential of protons in nuclei is the minimum energy required to add a proton to a nucleus at fixed neutron number. In terms of the proton and neutron chemical potentials, the beta-stability condition is expressed as

$$\mu_n = \mu_p + \mu_e \tag{2.2}$$

and also determines the electron chemical potential. Neutrinos are ignored because their mean-free path is longer than the radius of the star [4].

The number density of particle q (ρ_q) can be expressed in terms of the fermi momentum (k_q) as [3]

$$\rho_q = \frac{k_q^3}{3\pi^2}. \tag{2.3}$$

In ultra-dense matter electrons can attain ultra-relativistic energies and therefore it may become energetically more favourable to populate muon states. The appearance of muons requires a sufficiently high chemical potential of electrons, i.e. $\mu_e > m_\mu$, where m_μ is the mass of muons [29]. Muons have the same charge as an electron, but a mass of 104 MeV [4]. To calculate the core-crust transition density ρ_t, one only needs to deal with the *npe* matter since muons will normally not appear as the electron chemical potential μ_e is not high enough near ρ_t unless one uses an extremely soft symmetry energy [29].

Since the neutron star is assumed to be charge neutral, the number of protons must be equal to the number of electrons present. In terms of the Fermi momenta of the species this means that

$$k_e = k_p. \tag{2.4}$$

Eq. (2.2) together with Eq. (2.4) gives the corresponding proton fraction x_p as a function of baryon density.

2.3 Properties of symmetric nuclear matter constraining nuclear models

A key experimental constraint on the EOS is that the chosen potential reproduces the observed properties of nuclear matter at saturation. Although infinite nuclear matter is not directly observable, the equilibrium parameters of symmetric nuclear matter and some properties of asymmetric matter provide a physically plausible and intuitive way to characterize the bulk properties of a model.

2.3.1 Saturation density

Saturation means that no matter how many nucleons are added to nuclei, the central density will remain the same. This is due to the short range of the attractive nuclear force. But as more nucleon are added, the density increases, squeezing the nucleons together and when the distance between nucleons becomes smaller than 0.4 *fm*, the nuclear force becomes repulsive and the saturation density (ρ_0) is reached.

2.3.2 Symmetry energy

The symmetry energy describes how the energy of nuclear matter increases as the system departs from equal numbers of neutrons (N) and protons (Z). Hence, the symmetry energy determines the proton fraction in neutron star matter. The symmetry energy is given by [28]:

$$E_{sym} = \frac{1}{2}\left(\frac{\partial^2 \frac{E}{A}(\rho)}{\partial I^2}\right)_{I=0}, \qquad \left(I = \frac{\rho_n - \rho_p}{\rho}\right). \tag{2.5}$$

2.3.3 Incompressibility coefficient

The incompressibilty coefficient defines the curvature (a measure of how quickly a curve changes direction) of the equation of state at saturation.

The incompressibilty coefficient K is defined as [28]

$$K = 9\rho_0^2 \left(\frac{\partial^2 \frac{E}{A}}{\partial \rho^2} \right)_{\rho=\rho_0} . \tag{2.6}$$

2.3.4 Binding energy

Mathematically the binding energy is defined as $E_0 = \frac{E}{A}$. Energy is needed to separate a nucleus into its individual protons and neutrons, causing the separated nucleons to have a greater total rest energy than the rest energy of the original nucleus. This energy is called the binding energy and is positive. To form the nucleus again, energy must be released, in this case the binding energy is negative. In terms of neutron stars the binding energy is the energy released after the core of the original star collapses, thus assembling nucleons to form a neutron star.

2.4 Skyrme interactions

2.4.1 Description of the Skyrme interaction

The Skyrme interaction was first introduced by Skyrme in Refs. [33, 34] as a non-relativistic effective interaction for nuclear Hartree-Fock calculations that aims to parameterize the *t*-matrix for nucleon-nucleon scattering in the nuclear medium in a simple and efficient manner. Its widespread application started with the revival by Vautherin and Brink in Refs. [35, 36]. In the standard Skyrme Hartree-Fock (SHF) model, the interaction is taken to have a zero-range, density- and momentum-dependent form and the Skyrme interaction parameters are chosen to fit the binding energies and charge radii of a large number of nuclei in the periodic table. The Skyrme interaction has the following standard form:

$$
\begin{aligned}
V(\vec{r}_1,\vec{r}_2) = {} & t_0(1+x_0P_\sigma)\delta(\vec{r}) && \text{central term}\\
& + \tfrac{1}{2}t_1(1+x_1P_\sigma)\left[\vec{P}^{\dagger 2}\delta(\vec{r}) + \delta(\vec{r})\vec{P}^2\right] && \\
& + t_2(1+x_2P_\sigma)\vec{P}^{\dagger}\delta(\vec{r})\vec{P} && \text{non-local terms}\\
& + \tfrac{1}{6}t_3(1+x_3P_\sigma)\left[\rho\left(\vec{R}\right)\right]^{\sigma}\delta(\vec{r}) && \text{density-dependent term}\\
& + iW_0\vec{\sigma}\cdot\left[\vec{P}^{\dagger}\times\delta(\vec{r})\vec{P}\right] && \text{spin-orbit term}
\end{aligned}
\tag{2.7}
$$

where $\vec{r} = \vec{r}_1 - \vec{r}_2$, $\vec{R} = \frac{1}{2}(\vec{r}_1 + \vec{r}_2)$, $\vec{P} = \frac{1}{2i}\left(\vec{\nabla}_1 - \vec{\nabla}_2\right)$ is the relative momentum operator acting on the wave function to the right and $\vec{P}^{\dagger}$ is the adjoint of $\vec{P}$. $P_\sigma = \frac{1+\vec{\sigma}_1\cdot\vec{\sigma}_2}{2}$ is the spin-exchange operator and $\vec{\sigma} = \vec{\sigma}_1 + \vec{\sigma}_2$ the vector of Pauli spin matrices.

Within the standard form, Eq.(2.7), the total binding energy (ground-state energy) of a nucleus can be expressed as the integral of a density functional as follows [28]:

$$\langle\, \varphi \,\big|\, \hat{H} \,\big|\, \varphi \,\rangle = \int \mathcal{H}(\vec{r})\, dr, \tag{2.8}$$

with energy density $\mathcal{H}$;

$$\mathcal{H} = \mathcal{K} + \mathcal{H}_0 + \mathcal{H}_3 + \mathcal{H}_{\text{eff}} + \mathcal{H}_{\text{fin}} + \mathcal{H}_{\text{so}} + \mathcal{H}_{\text{sg}} + \mathcal{H}_{\text{Coul}}, \tag{2.9}$$

where $\mathcal{K} = \frac{\hbar^2}{2m}\tau$ is the kinetic energy term, $\mathcal{H}_0$ a zero-range term, $\mathcal{H}_3$ the density-dependent term, $\mathcal{H}_{\text{eff}}$ an effective-mass term, $\mathcal{H}_{\text{fin}}$ a finite-range term, $\mathcal{H}_{\text{so}}$ a spin-orbit term and $\mathcal{H}_{\text{sg}}$ a term due to the tensor coupling with spin and gradient. In $\mathcal{H}_{\text{Coul}}$ the exchange part can be calculated with the Slater approximation [28].

$$\mathcal{H}_0 = \frac{1}{4}t_0\left[(2+x_0)\rho^2 - (2x_0+1)\left(\rho_{\text{p}}^2 + \rho_{\text{n}}^2\right)\right],$$

$$\mathcal{H}_3 = \frac{1}{24}t_3\rho^{\sigma}\left[(2+x_3)\rho^2 - (2x_3+1)\left(\rho_{\text{p}}^2 + \rho_{\text{n}}^2\right)\right],$$

$$\mathcal{H}_{\text{eff}} = \frac{1}{8}[t_1(2+x_1) + t_2(2+x_2)]\tau\rho$$
$$+\frac{1}{8}[t_2(2x_2+1) - t_1(2x_1+1)]\left(\tau_{\text{p}}\rho_{\text{p}} + \tau_{\text{n}}\rho_{\text{n}}\right),$$

$$\mathcal{H}_{\text{fin}} = \frac{1}{32}[3t_1(2+x_1) - t_2(2+x_2)]\left(\vec{\nabla}\rho\right)^2$$
$$-\frac{1}{32}[3t_1(2x_1+1) + t_2(2x_2+1)]\left[\left(\vec{\nabla}\rho_{\text{p}}\right)^2 + \left(\vec{\nabla}\rho_{\text{n}}\right)^2\right],$$

$$\mathcal{H}_{\text{so}} = \frac{1}{2}W_0\left[\vec{J}\cdot\vec{\nabla}\rho + \vec{J}_{\text{p}}\cdot\vec{\nabla}\rho_{\text{p}} + \vec{J}_{\text{n}}\cdot\vec{\nabla}\rho_{\text{n}}\right],$$

$$\mathcal{H}_{\text{sg}} = -\frac{1}{16}(t_1x_1 + t_2x_2)\vec{J}^2 + \frac{1}{16}(t_1 - t_2)\left[\vec{J}_{\text{p}}{}^2 + \vec{J}_{\text{n}}{}^2\right],$$

$$\mathcal{H}_{\text{Coul}} = \mathcal{H}_{\text{Coul,dir}} + \mathcal{H}_{\text{Coul,exch}}$$

$$= \frac{e}{2}\rho_{\text{p}}(\vec{r})\int\frac{\rho_{\text{p}}(\vec{r}')}{|\vec{r}-\vec{r}'|}d^3r' - \frac{e^2}{2}\left(\frac{3}{\pi}\right)^{1/3}\rho_{\text{p}}{}^{4/3}. \qquad (2.10)$$

$\mathcal{H}_{\text{Coul,dir}}$ and $\mathcal{H}_{\text{Coul,exch}}$ are respectively the direct term and the exchange term of the Coulomb enegy density. Total densities are defined as $\rho = \rho_{\text{p}} + \rho_{\text{n}}$, $\tau = \tau_{\text{p}} + \tau_{\text{n}}$, $\vec{J} = \vec{J}_{\text{n}} + \vec{J}_{\text{p}}$. For the Skyrme interaction the energy density $\mathcal{H}(\vec{r})$ is an algebraic function of the nucleon densities ρ_{n} (ρ_{p}), the kinetic energy $\tau_{\text{n}}(\tau_{\text{p}})$, and isospin densities $\vec{J}_{\text{n}}(\vec{J}_{\text{p}})$, which in turn depend on the single-particle states φ_i^q defining the Slater-determinant wave function φ. Neutron and proton ($q = \text{n, p}$) local matter densities are:

$$\rho_{\text{q}}(\vec{r}) = \sum_{i,s}\left|\varphi_i^q(\vec{r},s)\right|^2 n_i^q, \qquad (2.11)$$

Similarly the kinetic and isospin densities read:

$$\tau_{\mathrm{q}}(\vec{r}) = \sum_{i,s} \left|\varphi_i^q(\vec{r},s)\right|^2 n_i^q \,, \tag{2.12}$$

$$\vec{J}_q(\vec{r}) = \sum_{i,s,s'} \varphi_i^{q\,*}(\vec{r},s')\,\vec{\nabla}\varphi_i^q(\vec{r},s) \times \langle s'|\vec{\sigma}|s\rangle n_i^q \,, \tag{2.13}$$

with orbital, spin and iso-spin quantum numbers, *i*, *s* and *q*, respectively and n_i^q is the occupation number of the corresponding state *i*, *s*, *q*. The sums are taken over all occupied single-particle states, thus $n_i^q = 1$. The expression for $\mathcal{H}(\vec{r})$ is derived explicitly in Ref. [35].

2.4.2 EOS with Skyrme interactions

Symmetric matter is represented by a Fermi gas in a volume Υ sufficiently large so that surface effects can be neglected. At zero temperature, the total energy per nucleon can be written in terms of the energy density, which is represented by the EOS, $\mathcal{E}(\rho)$ as [28]:

$$\frac{E}{A}(\rho) = \frac{\Upsilon}{A}\mathcal{E}(\rho) = \frac{\mathcal{E}(\rho)}{\rho} \,, \tag{2.14}$$

where E is the total energy of the system and A is the total baryon (nucleon) number. Each particle in the gas has a mean kinetic energy $\frac{3}{5}\mathcal{E}_F = \frac{3}{5}\frac{\hbar^2}{2m}k_F^2$, where $\mathcal{E}_F$ is the Fermi energy.

For symmetric nuclear matter $N = Z$ (equal number of neutrons, *N* and protons, *Z*):

$$\rho_{\mathrm{n}} = \rho_{\mathrm{p}} = \tfrac{1}{2}\rho, \qquad \tau_n = \tau_p = \tfrac{1}{2}\tau, \qquad \vec{J}_n = \vec{J}_p = \tfrac{1}{2}\vec{J} \,, \tag{2.15}$$

and in nuclear matter $\vec{\nabla}\rho = \vec{\nabla}\cdot\vec{J} = 0$.

In the case of a zero-range Skyrme force, the density functional (Eq. (2.9) and Eq. (2.10)) allows the energy per nucleon (binding energy) for infinite symmetric matter to be written as:

$$E_0 = \frac{E}{A}(\rho) = \frac{3\hbar^2}{10m}\left(\frac{3\pi^2}{2}\right)^{2/3}\rho^{2/3} + \frac{3}{8}t_0\rho + \frac{3}{80}\Theta_s\left(\frac{3\pi^2}{2}\right)^{2/3}\rho^{5/3} + \frac{1}{16}t_3\rho^{\sigma+1}\,. \qquad (2.16)$$

where $\Theta_s = [3t_3 + (5 + 4x_2)t_2]$.

As function of proton fraction $x_p = \frac{Z}{A}$ or iso-spin asymmetry $I = \frac{N-Z}{A}$, the density functional given by Eq.(2.9) and Eq.(2.10) can be used to write the energy per particle of asymmetric infinite nuclear matter:

$$\begin{aligned} E_b(\rho, I \text{ or } x_p) = {} & \frac{3\hbar^2}{10m}\left(\frac{3\pi^2}{2}\right)^{2/3}\rho^{2/3}F_{5/3} + \frac{1}{8}t_0\rho[2(x_0+2) - (2x_0+1)F_2] \\ & + \frac{1}{48}t_3\rho^{\sigma+1}[2(x_3+2) - (2x_3+1)F_2] + \frac{3}{40}\left(\frac{3\pi^2}{2}\right)^{2/3}\rho^{5/3} \\ & \times\left\{[t_1(x_1+2) + t_2(x_2+2)]F_{5/3} + \frac{1}{2}[t_2(2x_2+1) - t_1(2x_1+1)]F_{8/3}\right\}, \end{aligned} \qquad (2.17)$$

with the following definition for the asymmetry factors:

$$\begin{aligned} F_m(I) &= \frac{1}{2}[(1+I)^m + (1-I)^m], \\ F_m(x_p) &= 2^{m-1}\left[x_p^m + (1-x_p)^m\right]. \end{aligned} \qquad (2.18)$$

The underlying property, decisive for the validity of a Skyrme interaction in nuclear matter models, is the density dependence of the symmetry energy. By definition of Eq. (2.5) and using Eq. (2.17) , the symmetry energy can be written as:

$$E_{sym}(\rho) = \frac{1}{2}\left(\frac{\partial^2 E_b}{\partial I^2}\right)_{I=0}$$

$$= \frac{\hbar^2}{6m}\left(\frac{3\pi^2}{2}\right)^{2/3}\rho^{2/3} - \frac{1}{8}t_0(2x_0+1)\rho$$

$$-\frac{1}{24}\left(\frac{3\pi^2}{2}\right)^{2/3}\Theta_{sym}\rho^{5/3} - \frac{1}{48}t_3(2x_3+1)\rho^{\sigma+1} \qquad (2.19)$$

where $\Theta_{\mathrm{sym}} = 3\mathrm{t}_1\mathrm{x}_1 - \mathrm{t}_2(4+5\mathrm{x}_2)$. $\sigma, \mathrm{t}_0, \mathrm{t}_1, \mathrm{t}_2, \mathrm{t}_3,\ \mathrm{x}_0, \mathrm{x}_1, \mathrm{x}_2$ and x_3 are the Skyrme parameters.

The pressure in the neutron star matter is [28]

$$P = -\frac{\partial E}{\partial V}\Big|_A = \frac{A}{V^2}\frac{\partial E}{\partial \rho}\Big|_A = \rho^2 \frac{\partial \frac{E}{A}(\rho)}{\partial \rho}\Bigg|_A . \qquad (2.20)$$

By taking the derivative of the energy per nucleon (Eq. 2.16) with respect to the baryon density, the pressure is obtained

$$P(\rho) = \rho\left\{\frac{\hbar^2}{5m}\left(\frac{3\pi^2}{2}\right)^{2/3}\rho^{2/3} + \frac{3}{8}t_0\rho + \frac{1}{16}\Theta_s\left(\frac{3\pi^2}{2}\right)^{2/3}\rho^{5/3} + \frac{1}{16}t_3(\sigma+1)\rho^{\sigma+1}\right\}. \qquad (2.21)$$

At the saturation density (ρ_0) the pressure equals zero and Eq. (2.21) satisfies the following equation, giving the definition of the saturation density

$$P = \rho_0^2\left(\frac{d}{d\rho}\frac{E}{A}(\rho)\right)_{\rho=\rho_0} = 0. \qquad (2.22)$$

By definition (2.6) the incompressibility coefficient can be written as

$$K = 9\rho_0^2 \left(\frac{\partial^2 \frac{E}{A}}{\partial \rho^2} \right)_{\rho=\rho_0}$$

$$= -\frac{3\hbar^2}{5m}\left(\frac{3\pi^2}{2}\right)^{2/3}\rho_0^{2/3} + \frac{3}{8}\Theta_s\left(\frac{3\pi^2}{2}\right)^{2/3}\rho_0^{5/3} + \frac{9}{16}\sigma(\sigma+1)t_3\rho_0^{\sigma+1}. \quad (2.23)$$

The relation between the symmetry energy and the slope L and the curvature K_{sym} of the symmetry energy at ρ_0 is defined by the following equations.

$$L = 3\rho_0 \left. \frac{\partial E_{sym}(\rho)}{\partial \rho} \right|_{\rho=\rho_0}$$

$$= \frac{\hbar^2}{3m}\left(\frac{3\pi^2}{2}\right)^{2/3}\rho_0^{2/3} - \frac{3}{8}t_0(2x_0+1)\rho_0$$

$$-\frac{5}{24}\left(\frac{3\pi^2}{2}\right)^{2/3}\Theta_{\mathrm{sym}}\rho_0^{5/3} - \frac{1}{16}(\sigma+1)t_3(2x_3+1)\rho_0^{\sigma+1} \quad (2.24)$$

$$K_{sym} = 9\rho_0^2 \left. \frac{\partial^2 E_{sym}(\rho)}{\partial \rho^2} \right|_{\rho=p_0}$$

$$-\frac{1}{3m}\left(\frac{3\pi^2}{2}\right)^{2/3}\rho_0^{2/3} - \frac{5}{12}\left(\frac{3\pi^2}{2}\right)^{2/3}\Theta_{\mathrm{sym}}\rho_0^{5/3} - \frac{3}{16}\sigma(\sigma+1)t_3(2x_3+1)\rho_0^{\sigma+1}. \quad (2.25)$$

2.4.3 Skyrme parameters

In his original work Skyrme fixed the numerical values of the parameters by fitting the binding energy and density of nuclear matter and also binding energies and mass differences of some light nuclei calculated with oscillator wave functions [36]. Different groups have different biases in selecting the observables they want to reproduce. Fits are usually restricted to a few semi- or doubly-magic spherical nuclei. All fits take care of binding energy and root mean square (r.m.s.) charge radii after which different tracks are pursued. Pairing properties are usually adjusted to the odd–even staggering of binding energies. Some fits add information on nuclear matter, others

make a point to include information from the electromagnetic form factor. Differences exist also in the bias and weight given to the various observables. In view of these different prejudices entering the fits, there exists many different parameterizations for Skyrme Hartree-Fock (SHF) [29].

The values of Skyrme parameters used in this work are taken from Refs. [8, 11, 12, 13, 28, 29, 37, 38, 39] and are given in Table 2.1. The fifteen Skyrme interactions used in this project are those most commonly used in the literature.

Skyrme	t_0	t_1	t_2	t_3	x_0	x_1	x_2	x_3	σ
SIII	-1128.75	395.00	-95.00	14000.00	0.45	0.00	0.00	1.00	1.00
SKP	-2931.70	320.62	-337.41	18708.96	0.292	0.653	-0.537	0.181	1/6
SLy230a	-2490.23	489.53	-566.58	13803.00	1.1318	-0.8426	-1.0	1.9219	1/6
Sly230b	-2488.91	486.82	-546.39	13777.00	0.8340	-0.3438	-1.0	1.3539	1/6
SKM*	−2645.00	410.00	−135.00	15595.00	0.09	0.00	0.00	0.00	1/6
SKM	−2645.00	385.00	-120.00	15595.00	0.09	0.00	0.00	0.00	1/6
SKXm	-1445.30	246.90	-131.80	12103.90	0.340	0.580	0.127	0.030	0.50
SKI3	−1762.88	561.61	−227.09	8106.20	0.308	−1.172	−1.091	1.293	0.25
SKI4	−1855.83	473.83	1006.86	9703.61	0.405	−2.889	−1.325	1.145	0.25
SLy6	−2479.50	462.18	−448.61	13673.00	0.825	−0.465	−1.000	1.355	1/6
BSK1	−1830.45	262.97	−296.45	13444.70	0.600	−0.500	−0.500	0.823	1/3
SGII	-2645.00	340.00	-41.90	15595.00	0.090	-0.0588	1.4250	0.0604	1/6
SKX	-1445.30	246.90	-131.80	12103.90	0.340	0.580	0.127	0.030	0.5
SKXce	-1438.00	244.30	-133.70	12116.30	0.288	0.611	0.145	-0.056	0.5
SkSC4	-1789.40	283.50	-283.5	12782.30	0.79	-0.50	-0.50	1.139	1/3

Table 2.1: Parameters of the Skyrme forces used in project. t_0 is in $MeVfm^3$, t_1, t_2 are in $MeVfm^5$, t_3 is in $MeVfm^{3+3\sigma}$. All other parameters are dimensionless.

2.5 The EOS and symmetry energy with the modified Gogny interaction (MDI)

In 1980 Dechargé and Gogny proposed a parametrization for an effective nuclear interaction called the Gogny interaction. By using the Hartree-Fock calculation they expressed the baryon potential energy density as [40]

$$V(\rho, I) = \frac{A_u(x)\rho_n\rho_p}{\rho_0} + \frac{A_l(x)}{2\rho_0}\left(\rho_n^2 + \rho_p^2\right) + \frac{B}{\sigma+1}\frac{\rho^{\sigma+1}}{\rho_0^{\sigma}}(1 - xI^2)$$

$$+\frac{1}{\rho_0}\sum_{\tau,\tau'} C_{\tau,\tau'}\iint d^3k\, d^3k' \frac{f_\tau(\vec{r},\vec{k}) f_{\tau'}(\vec{r},\vec{k}')}{1 + \left(\vec{k} - \vec{k}'\right)^2/\Lambda^2}\,. \tag{2.26}$$

The Gogny interaction has become popular for calculating the EOS of pure neutron matter and describing finite nuclei. It has also found use in a variety of studies which include heavy-ion reactions, liquid-gas phase transitions in neutron-rich matter and several structural properties and gravitational wave emissions of neutron stars.

The single particle potential $U\left(\rho, I, \vec{k}, \tau\right)$ for a nucleon is found by taking the derivative of Eq. (2.26) with respect to the proton or neutron density resulting in:

$$U\left(\rho, I, \vec{k}, \tau\right) = A_u(x)\frac{\rho_{-\tau}}{\rho_0} + A_l(x)\frac{\rho_\tau}{\rho_0} + B\left(\frac{\rho}{\rho_0}\right)^{\sigma}(1 - xI^2) - 8\tau x\frac{B}{\sigma+1}\frac{\rho^{\sigma-1}}{\rho_0^{\sigma}} I\rho_{-\tau}$$

$$+\frac{2C_{\tau,\tau}}{\rho_0}\int d^3k' \frac{f_\tau\left(\vec{r},\vec{k}'\right)}{1 + \left(\vec{k} - \vec{k}'\right)^2/\Lambda^2} + \frac{2C_{\tau,-\tau}}{\rho_0}\int d^3k' \frac{f_{-\tau}\left(\vec{r},\vec{k}'\right)}{1 + \left(\vec{k} - \vec{k}'\right)^2/\Lambda^2}\,, \tag{2.27}$$

which is dependent on the nucleon momentum $\vec{k}$ and isospin τ = 1/2 for neutrons and τ = -1/2 for protons. The single particle potential aswell as the coefficients $A_u(x)$ and $A_l(x)$ depend on the parameter x, which is brought in to compensate for the differing behaviour of the symmetry

energy above saturation density (which is model dependent), without changing the properties of symmetric nuclear matter. The symmetry energy at the saturation density $E_{sym}(\rho_0)$ will also remain unaffected by x. The values of these coefficients are $A_u(x) = -95.98 - x\frac{2B}{\sigma+1}$ and $A_l(x) = -120.57 + x\frac{2B}{\sigma+1}$. By chosing $x = 1$ the symmetry energy will begin to decrease after the saturation density, showing a downward bend in the symmetry energy versus baryon density curve. By chosing $x = 0$ the symmetry energy will continue to rise as a fuction of baryon density. By using definition (2.5) the symmetry energy at saturation ($\rho_0 = 0.16\, fm^{-3}$) is found to be $30.54\, MeV$.

Other parameter values are $\sigma = 4/3$, $B = 106.35\, MeV$, $C_{\tau,\tau} = -11.70\, MeV$, $C_{\tau,-\tau} = -103.40\, MeV$ and $\Lambda = \rho_0^f$ which is the Fermi momentum of nuclear matter at saturation density ρ_0. For simplicity in calculations define $C_{1/2,1/2} = C_{-1/2,-1/2} = C_{like}$ and $C_{1/2,-1/2} = C_{-1/2,1/2} = C_{unlike}$.

The constants appearing in Eq. (2.26) are fixed by ensuring that properties of cold nuclear matter are reproduced. By writing the phase space distribution function at zero temperature as $f_\tau(\vec{r},\vec{k}) = \left(\frac{2}{h^3}\right)\Theta\left[k_f(\tau) - k\right]$, all the integral expressions can be calculated analytically. The integration in Eq. (2.26) is facilitated by noting that for a fixed $\vec{k} \equiv \frac{(\vec{k}_1 - \vec{k}_2)}{2}$, the center of mass momentum can be integrated out to give

$$\int_0^{k_f(\tau)} \int_0^{k_f(\tau')} d^3k_1\, d^3k_2 s(\vec{k})$$

$$= \int_0^{q_f} \left[\frac{16\pi}{3}\left[k_f^3(\tau) + k_f^3(\tau')\right] - 8\pi k\left[k_f^2(\tau) + k_f^2(\tau')\right]\right.$$

$$\left. + \frac{16\pi}{3}k^3 - \frac{\pi}{k}\left[k_f^2(\tau) - k_f^2(\tau')\right]^2\right] s(\vec{k}) d^3k, \qquad (2.28)$$

where $q_f = \frac{k_f(\tau) + k_f(\tau')}{2}$.

$$\int d^3k' \frac{f_\tau(\vec{r},\vec{k}')}{1+\left(\vec{k}-\vec{k}'\right)^2/\Lambda^2}$$

$$= \frac{2}{h^3}\pi\Lambda^3\left[\frac{k_f^2(\tau)+\Lambda^2-k^2}{2k\Lambda} ln\frac{\left[k+k_f(\tau)\right]^2+\Lambda^2}{\left[k-k_f(\tau)\right]^2+\Lambda^2}\right.$$

$$\left.+\frac{2k_f(\tau)}{\Lambda}-2\left\{arctan\left(\frac{k+k_f(\tau)}{\Lambda}\right)-arctan\left(\frac{k-k_f(\tau)}{\Lambda}\right)\right\}\right], \quad (2.29)$$

$$\iint d^3k\, d^3k' \frac{f_\tau(\vec{r},\vec{k}) f_{\tau'}(\vec{r},\vec{k}')}{1+\left(\vec{k}-\vec{k}'\right)^2/\Lambda^2}$$

$$= \frac{1}{6}\left(\frac{4\pi}{h^3}\right)^2\Lambda^2\left\{k_f(\tau)k_f(\tau')\left[3\left(k_f^2(\tau)+k_f^2(\tau')\right)-\Lambda^2\right]\right.$$

$$+4\Lambda\left[\left(k_f^3(\tau)-k_f^3(\tau')\right)arctan\left(\frac{k_f(\tau)-k_f(\tau')}{\Lambda}\right)-\left(k_f^3(\tau)+k_f^3(\tau')\right)arctan\left(\frac{k_f(\tau)+k_f(\tau')}{\Lambda}\right)\right]$$

$$\left.+\frac{1}{4}\left[\Lambda^4+6\Lambda^2\left(k_f^2(\tau)+k_f^2(\tau')\right)-3\left(k_f^2(\tau)-k_f^2(\tau')\right)^2\right]\times ln\frac{\left(k_f(\tau)+k_f(\tau')\right)^2+\Lambda^2}{\left(k_f(\tau)-k_f(\tau')\right)^2+\Lambda^2}\right\}. \quad (2.30)$$

The kinetic energy is

$$E_k(\rho,I) = \frac{1}{\rho}\int d^3p\left(\frac{k^2}{2m}f_n(\vec{r},\vec{k})+\frac{k^2}{2m}f_p(\vec{r},\vec{k})\right)$$

$$= \frac{4\pi}{5mh^3}\left(k_n^5+k_p^5\right). \quad (2.31)$$

where $k_{n(p)} = \hbar\left(3\pi^2\rho_{n(p)}\right)^{1/3}$ is the Fermi momentum of neutrons (protons). By adding the potential energy and kinetic energy the total energy per baryon for cold asymmetric nuclear matter is found

$$E_b(\rho, I) = \frac{V(\rho, I)}{\rho} + E_k(\rho, I). \tag{2.32}$$

By setting $\rho_n = \rho_p = \frac{\rho}{2}$ and $k_n = k_p = k_f$ one finds the following EOS for cold symmetric nuclear matter

$$E_0(\rho) = \frac{8\pi}{5mh^3\rho}k_f^5 + \frac{\rho}{4\rho_0}\left(A_l(x) + A_u(x)\right) + \frac{B}{\sigma+1}\frac{\rho}{\rho_0}^{\sigma} + \frac{1}{3\rho_0\rho}(C_l + C_u)\left(\frac{4\pi}{h^3}\right)^2\Lambda^2$$

$$\times\left[k_f^2\left(6k_f^2 - \Lambda^2\right) - 8\Lambda k_f^3 arctan\left(\frac{2k_f}{\Lambda}\right) + \frac{1}{4}\left(\Lambda^4 + 12\Lambda^2k_f^2\right)ln\frac{4k_f^2 + \Lambda^2}{\Lambda^2}\right]. \tag{2.33}$$

Since $A_l(x) + A_u(x)$ is a constant of $-216.55\ MeV$, the EOS is independent of x, allowing one to calculate symmetric nuclear matter properties at saturation. The big question is what happens above saturation, this will be dealt with in chapter 4.

From the definition of the symmetry energy:

$$E_{sym}(\rho) = \frac{1}{2}\left(\frac{\partial^2 E_b}{\partial I^2}\right)_{I=0}$$

$$= \frac{8\pi}{9mh^3\rho}k_f^5 + \frac{\rho}{4\rho_0}\left(A_l(x) - A_u(x)\right) - \frac{Bx}{\sigma+1}\left(\frac{\rho}{\rho_0}\right)^{\sigma}$$

$$+ \frac{C_l}{9\rho_0\rho}\left(\frac{4\pi}{h^3}\right)^2\Lambda^2\left[4k_f^4 - \Lambda^2k_f^2 ln\frac{4k_f^2 + \Lambda^2}{\Lambda^2}\right]$$

$$+ \frac{C_u}{9\rho_0\rho}\left(\frac{4\pi}{h^3}\right)^2\Lambda^2\left[4k_f^4 - k_f^2\left(4k_f^2 + \Lambda^2\right)ln\frac{4k_f^2 + \Lambda^2}{\Lambda^2}\right], \tag{2.34}$$

where $k_f = \hbar\left(3\pi^2\frac{\rho}{2}\right)^{1/3}$ is the Fermi momentum for symmetric nuclear matter. Since $A_l(x) - A_u(x) = -24.59 + \frac{4Bx}{\sigma+1}$, the symmetry energy becomes linear in x at a certain density except ofcourse at saturation.

2.6 Summary

The aim of this chapter was to introduce the models used in this work for describing nuclear matter through the EOS. Equilibrium conditions and properties of nuclear matter at saturation were also discussed. The focus was on the Skyrme interaction and its parameter sets, the modified Gogny interaction was also introduced and serves as another way to describe nuclear matter for undertaking in a PhD project. The next chapter shows how these two interactions can be used to locate the crust-core transition density within two methods called the dynamical method and the thermodynamical method.

CHAPTER 3

Methods for locating the inner edge of a neutron star crust

3.1 Introduction

A well established approach for estimating the transition density (ρ_t) is to search for the density at which the uniform liquid in the core first becomes unstable against small-amplitude density fluctuations, indicating the start of forming nuclear clusters [8, 40, 41]. In other words, the system is separated into two macroscopic (infinite) phases of different densities. In this chapter a description of two such methods, namely the dynamical method and the thermodynamical method, is given. The neutron star is assumed to be static, spherical symmetric, consisting of electrons and non-relativistic neutrons and protons in beta-equilibrium, under the constraint of charge neutrality, at temperature $T = 0\ MeV$.

3.2 Dynamical method

The instability region of homogeneous neutron, proton and electron matter against clusterization is determined by studying how the system's free-energy (the total energy needed to create the system) changes when a finite-size density fluctuation is introduced. If fluctuations occur on a finite microscopic scale, electron and proton densities can fluctuate independently, only their mean values are constrained to be equal, insuring macroscopic charge neutrality. Fluctuations thus affect independently the three species of the medium (neutrons, protons and electrons), whose densities become [40]:

$$\rho_q = \rho_q^0 + \delta\rho_q \tag{3.1}$$

with $q \in \{n, p, e\}$. Each density variation can be expressed by a Fourier transform

$$\delta\rho_q = \int d\vec{k} a_q(\vec{k}) e^{i\vec{k}\cdot\vec{r}}, \tag{3.2}$$

with $a_q(\vec{k}) = a_q^*(-\vec{k})$ to ensure that $\delta\rho_q$ is real. Since the different wave vectors $\vec{k}$ are decoupled in the global free-energy variation, the problem reduces to the study of plane-wave density fluctuations:

$$\delta\rho_q = A_q e^{i\vec{k}\cdot\vec{r}} + complex\ conjugate, \tag{3.3}$$

where each species is associated with a different amplitude. This kind of density variation occurs when a momentum $\vec{k}$ is transferred to the particle system, i.e. through collisions and the "dynamical method" is named after this.

To evaluate the free-energy variation, consider a Thomas-Fermi approximation, i.e. the density variation is supposed smooth enough to allow at each point the definition of a Fermi sphere corresponding to the local density. Then, at each point of density $\rho_q(\vec{r}) = \rho_q^0 + \delta\rho_q$, the local bulk term of the free-energy is equal to the free-energy f^h of an infinite homogeneous system at the same density. The global bulk free-energy of the system is the space average of this local term:

$$f^b = \frac{1}{V}\int f^h(\{\rho_q(\vec{r})\})d\vec{r}\ . \tag{3.4}$$

In the small-amplitude limit, the integration leads to $f^b = f^h(\{\rho_q^0\}) + \delta f^b$, with

$$\delta f^b = \sum_{i,j} \frac{A_i A_j^* + A_i^* A_j}{2}\left(\frac{\partial^2 f^h}{\partial\rho_i\partial\rho_j}\right)_{\{\rho_q^0\}} = \sum_{i,j} \frac{A_i A_j^* + A_i^* A_j}{2}\left(\frac{\partial\mu_j}{\partial\rho_j}\right)_{\{\rho_q^0\}}, \tag{3.5}$$

where $i,j\,\epsilon\,\{n,p,e\}$. First-order terms have vanished in the integration because the average density variation is zero.

The variation of the entropy is contained in the bulk term, since entropy depends only on the local density. However, in the case of a finite wave number k, the energy density is modified by two additional terms, arising from the density-gradient dependence of the nuclear force, and from the Coulomb interaction. Denoting these two contributions $\delta\mathcal{E}^{\nabla}$ and $\delta\mathcal{E}^{c}$ respectively, the free-energy variation is:

$$\delta f = \delta f^{b} + \delta\mathcal{E}^{\nabla} + \delta\mathcal{E}^{c}. \tag{3.6}$$

In the presence of density gradients the nuclear energy density has the form $\mathcal{H} = \mathcal{H}^{h} + \mathcal{H}^{\nabla}$, where $\mathcal{H}^{h}$ is given by Eq. (2.9) and the density-gradient term $\mathcal{H}^{\nabla}$ is expressed as:

$$\mathcal{H}^{\nabla} = D_{nn}(\nabla\rho_n)^2 + D_{pp}\left(\nabla\rho_p\right)^2 + 2D_{np}\nabla\rho_n \cdot \nabla\rho_p. \tag{3.7}$$

Coefficients D_{ij} are combinations of the Skyrme parameters:

$$D_{nn} = D_{pp} = \tfrac{3}{16}[t_1(1-x_1) - t_2(1+x_2)], \tag{3.8}$$

$$D_{np} = D_{pn} = \tfrac{1}{16}[3t_1(2+x_1) - t_2(2+x_2)], \tag{3.9}$$

where t_1, t_2, x_1, x_2 are Skyrme parameters. The MDI interaction, however, does not have a gradient term. By letting $D_{nn} = D_{pp} = D_{np} = 132\ MeVfm^5$ this drawback is overcome,as used in Ref. [10] when the MDI interaction is applied.

The global contribution of this term to the energy density is given by the space average:

$$\delta\mathcal{E}^{\nabla} = \frac{1}{V}\int \mathcal{H}^{\nabla}(\vec{r})d\vec{r} = k^2\sum_{i,j}\left(A_iA_j^{*} + A_i^{*}A_j\right)D_{ij}\ , \tag{3.10}$$

where $i, j \in \{n, p\}$.

The Coulomb contribution $\delta\mathcal{H}^c$ is due to the independent density fluctuations of charged particles $\{e,p\}$. Denoting $e_i = \frac{q_i}{\sqrt{4\pi\epsilon_0}}$, with q_i the electric charge of a particle of type i, this creates the charge distribution ρ_c:

$$\rho_c(\vec{r}) = \sum_i e_i A_i e^{i\vec{k}\cdot\vec{r}} + complex\ conjugate. \tag{3.11}$$

The consequent Coulomb energy per unit volume is:

$$\delta\mathcal{E}^c = \frac{1}{2V}\int \frac{\rho_c(\vec{r}_1)\rho_c(\vec{r}_2)}{|\vec{r}_2 - \vec{r}_1|}\, d\vec{r}_1\, d\vec{r}_2$$

$$= \frac{4\pi e_i e_j}{k^2}\sum_{i,j}\frac{A_i A_j^* + A_i^* A_j}{2}, \tag{3.12}$$

where $i,j\ \epsilon\ \{e,p\}$.

Summing the contributions (3.5), (3.10) and (3.12), gives the total free-energy variation, expressed to the second order in A_q:

$$\delta f = \sum_{i,j}\frac{A_i A_j^* + A_i^* A_j}{2}\left[\left(\frac{\partial\mu_i}{\partial\rho_j}\right)_{\{\rho_q^0\}} + 2D_{ij}\ \mathrm{k}^2 + \frac{4\pi e_i e_j}{k^2}\right], \tag{3.13}$$

which can be written in a matrix form in the three-dimensional space of density fluctuations $\tilde{A} = (A_n, A_p, A_e)$:

$$\delta f = \tilde{A}^* C^f \tilde{A}, \tag{3.14}$$

where

$$C^f = \begin{pmatrix} \frac{\partial \mu_n}{\partial \rho_n} & \frac{\partial \mu_n}{\partial \rho_p} & 0 \\ \frac{\partial \mu_p}{\partial \rho_n} & \frac{\partial \mu_p}{\partial \rho_p} & 0 \\ 0 & 0 & \frac{\partial \mu_e}{\partial \rho_e} \end{pmatrix} + k^2 \begin{pmatrix} 2D_{nn} & 2D_{np} & 0 \\ 2D_{pn} & 2D_{pp} & 0 \\ 0 & 0 & 0 \end{pmatrix} + \frac{4\pi e^2}{k^2} \begin{pmatrix} 0 & 0 & 0 \\ 0 & 1 & -1 \\ 0 & -1 & 1 \end{pmatrix} \tag{3.15}$$

is the free-energy curvature matrix and e is the elementary electric charge. The first term is the bulk term, which defines the stability condition of the nuclear matter (homogeneous nuclear matter plus electron gas) part. The density-gradient part of the nuclear interaction adds a term proportional to k^2, while the Coulomb interaction induced by the plane-wave charge distribution adds a term inversely proportional to k^2.

The region of instability of homogeneous matter against clusterization can be defined following a static relation: the homogeneous system will be considered unstable if the introduced density fluctuation reduces the total free-energy. Thus, the homogeneous matter will become unstable if the variation of the free-energy density becomes negative (Eq. (3.14)). This is obviously equivalent to saying that the homogeneous matter is stable if the variation of the free-energy density is zero. From thermodynamics, it is known that the free-energy curvature matrix is positive definite (shown in section 3.3), if the matter is thermodynamically stable (in this work the neutron star matter is assumed to be in thermodynamic equilibrium). This implies that the variation of the free-energy density is positive definite (from the definition of positive definiteness in Ref. [42]), meaning that $\delta f > 0$. Since C^f is symmetric, it will be positive definite if and only if all the eigenvalues are positive [42]. A necessary and sufficient condition for C^f to have positive eigenvalues is that a number of minors of the determinant be positive [42, 8]:

$$C^f_{11} > 0 \text{ or } C^f_{22} > 0, \begin{vmatrix} C^f_{11} & C^f_{12} \\ C^f_{21} & C^f_{22} \end{vmatrix} > 0, \begin{vmatrix} C^f_{11} & C^f_{12} & C^f_{13} \\ C^f_{21} & C^f_{22} & C^f_{23} \\ C^f_{31} & C^f_{32} & C^f_{33} \end{vmatrix} > 0. \tag{3.16}$$

This gives the condition for stability. Here C_{33}^{f} is always positive and is thus not taken into consideration. In the case of the problem under consideration, the first two conditions correspond to the requirement that the system be stable with respect to small modulations of the proton and neutron density respectively, and the third is a requirement for simultaneous modulations of proton and neutron densities. The final condition involves modulation of all three densities.

For all of the nuclear interactions employed here, the diagonal terms of the matrix are positive. The most stringent condition for stability is then the requirement that the determinant of the whole matrix be positive, since the determinant of the 2 x 2 neutron-proton part of the matrix is always greater than the determinant of the whole matrix.

The condition that the determinant be positive can be written as

$$V_{dyn}(k) = \left(\frac{\partial \mu_p}{\partial \rho_p} + D_{pp}k^2 + \frac{4\pi e^2}{k^2}\right) - \frac{\left(\partial \mu_p/\partial \rho_n + D_{pn}k^2\right)^2}{\partial \mu_n/\partial \rho_n + D_{nn}k^2}$$

$$- \frac{\left(4\pi e^2/k^2\right)^2}{\partial \mu_e/\partial \rho_e + D_{ee}k^2 + 4\pi e^2/k^2} > 0. \qquad (3.17)$$

$V_{dyn}(k)$ is the potential of the effective interaction between protons and represents the tendency to stability of the protons; the terms in the first bracket are the nuclear bulk, density gradient, and Coulomb contributions to the direct interaction of the proton modulations. The second and third terms are the induced effects due to the interactions of the proton modulations with those of the neutrons and the electrons, respectively. Approximations to these latter terms obtained by neglecting D_{ee} and all but the lowest powers of D_{nn} and D_{np} bring these terms into the form discussed in Ref. [43] :

$$V_{dyn}(k) = V_0 + \beta k^2 + \frac{4\pi e^2}{k^2 + k_{TF}^2} > 0, \qquad (3.18)$$

where

$$V_0 = \frac{\partial \mu_p}{\partial \rho_p} - \frac{\left(\partial \mu_n / \partial \rho_p\right)^2}{\partial \mu_n / \partial \rho_n}\,, \tag{3.19}$$

$$\beta = D_{pp} + 2D_{np}\zeta + \upsilon D_{nn}\zeta^2\,, \quad \zeta = -\frac{\partial \mu_p / \partial \rho_n}{\partial \mu_n / \partial \rho_n}\,, \tag{3.20}$$

$$k_{TF}^2 = \frac{4\pi e^2}{\partial \mu_e / \partial \rho_e}\,. \tag{3.21}$$

In the above expressions the relation $\frac{\partial \mu_n}{\partial \rho_p} = \frac{\partial \mu_p}{\partial \rho_n}$ is used, following $\frac{\partial \mu_n}{\partial \rho_p} = \frac{\partial}{\partial \rho_p}\left(\frac{\partial \mathcal{E}}{\partial \rho_n}\right) = \frac{\partial}{\partial \rho_n}\left(\frac{\partial \mathcal{E}}{\partial \rho_p}\right) = \frac{\partial \mu_p}{\partial \rho_n}$ with $\mathcal{E}$ being the energy density of *npe* matter. Meanwhile, $\frac{\partial \mu_n}{\partial \rho_n}$ is assumed to be positive. Conversely if $\frac{\partial \mu_n}{\partial \rho_n} < 0$ but $\frac{\partial \mu_p}{\partial \rho_p} > 0$ the form of the equations changes correspondingly. In the current situation where k_{TF}^2 is small compared with k^2, the gradient and the Coulomb terms make approximately equal contributions to $V_{dyn}(k)$ thus helping to make the system more stable. There is a minimal value $V_{dyn}(Z)$ at $k = Z$ that marks the least stable modulation

$$Z = \left[\left(\frac{4\pi e^2}{\beta}\right)^{1/2} - k_{TF}^2\right]^{1/2}\,, \tag{3.22}$$

$$V_{dyn}(Z) = V_0 + 2(4\pi e^2 \beta)^{1/2} - \beta k_{TF}^2\,. \tag{3.23}$$

Then the density at which Eq. (3.23) becomes zero determines the instability boundary.

3.3 Thermodynamical method

The thermodynamic state of a given phase is described by two conserved quantities (at thermodynamic- and beta-equilibrium): baryon number B and charge Q, where Q is the sum over all charge carriers $Q = -N_p + N_e + N_\mu + \cdots$, where N_i is the number of each particle type. This quantity Q, which is introduced with the opposite sign from usual, is positive for negative charge carriers and so the chemical potential corresponding to Q is just the electron chemical potential μ_e a fundamental quantity in beta-equilibrium matter. Considering a phase with volume V, its total energy U is a function of the conserved quantities V, B and Q, i.e., $U = U(V, B, Q)$. It is easier to investigate the intrinsic stability of a single phase by introducing intensive quantities rather than extensive quantities, dividing by the baryon number

$$u = \frac{U}{B}\,, \quad v = \frac{V}{B}\,, \quad g = \frac{Q}{B} \tag{3.24}$$

then the energy per baryon becomes a function of two variables

$$u = u(v, g) \tag{3.25}$$

and the first law of thermodynamics at temperature $T = 0$ takes the form

$$du = -Pdv + \mu dg\,. \tag{3.26}$$

From Eq. (3.26) the total pressure of the *npe* system can be written as $P = P_b + P_e$ with the contributions P_b and P_e from baryons and electrons, respectively and μ the chemical potential of electric charge, given by

$$P = -\left(\frac{\partial u}{\partial v}\right)_g\,, \quad \mu = \left(\frac{\partial u}{\partial g}\right)_v \tag{3.27}$$

or

$$P = -\left(\frac{\partial u}{\partial v}\right)_{\mu} , \quad \mu = \left(\frac{\partial u}{\partial g}\right)_{P} . \tag{3.28}$$

From the principle of minimum energy, it can be deduced that the phase is intrinsically stable (i.e., it does not separate into different phases) if and only if the energy per baryon is a convex function of its variables v and g.

Consider the stability conditions for a homogeneous single-component fluid system, Ω, in a state characterized by U, V and N. The entropy is given by the fundamental relation $S = S(U, V, N)$.

The principle of maximum entropy states the following postulates, which are equivalent to the usual statement of the second law of thermodynamics [44, 45]:

(i) For a system at equilibrium, there exists a positive differentiable entropy function $S(U, V, N)$. As a general rule, this function is an increasing function of U for fixed V and N.

(ii) For a system made of M subsystems, S is additive, or extensive: the total entropy S_{tot} is the sum of the entropies of the subsystems,

$$S_{tot} = \sum_{m=1}^{M} S(U_m, V_m, N_m). \tag{3.29}$$

(iii)Suppose the global isolated system is initially divided by internal constraints into subsystems that are separately at equilibrium: if one (or more) constraint is lifted, the final entropy, after the re-establishment of equilibrium must be greater than or equal to the initial entropy. The new values of (U_m, V_m, N_m) are such that the entropy can only increase or stay unchanged. In summary: the entropy of an isolated system cannot decrease.

From the maximum entropy principle, Ω will be in a stable state provided there is no other state having greater entropy for the same values of U, V and N. Suppose, for instance that it is possible to divide Ω into two subsystems, Ω_a and Ω_b, such that,

$$S(U_a, V_a, N_a) + S(U_b, V_b, N_b) > S(U, V, N)$$

where $U = U_a + U_b$, $V = V_a + V_b$ and $N = N_a + N_b$ [44, 45]. In that case the original state will be unstable so that the system will tend to separate into subsystems in order to maximize $S(U_a, V_a, N_a) + S(U_b, V_b, N_b)$. That process would represent a phase change and, in general, the partitioned system would not be homogeneous. Thus, in order for the fluid to be stable against such an internal process it is necessary that

$$S(U_a + U_b, V_a + V_b, N_a + N_b) \geq S(U_a, V_a, N_a) + S(U_b, V_b, N_b), \tag{3.30}$$

for all U_a, V_a, N_a and U_b, V_b, N_b.

The minimum energy principle states that at equilibrium the energy of the composite system U_c is minimized subject to the entropy of the composite system S_c being constant [44, 45]. According to this principle there will be a corresponding condition in the energy representation. This condition can be established formally from Eq. (3.30).

Consider a partitioning of Ω into subsystems Ω_a and Ω_b such that the entropy of Ω, $S = S_a + S_b$, as well as *V* and *N*, is constant. The energy of Ω may not be the same in the partitioned as in the homogeneous unpartitioned state. In the homogeneous state, the energy U_h, is given by

$$U_h = U(S, V, N) = U(S_a + S_b, V_a + V_b, N_a + N_b)\,, \tag{3.31}$$

and in the unpartitioned state the energy is $U_a + U_b$, where

$$U_a = U(S_a, V_a, N_a)\,, \qquad U_b = U(S_b, V_b, N_b)\,. \tag{3.32}$$

Since the entropy of the homogeneous and the inhomogeneous states of Ω is the same,

$$S(U_h, V_a + V_b, N_a + N_b) = S(U_a, V_a, N_a) + S(U_b, V_b, N_b) \tag{3.33}$$

and it then follows from Eq. (3.30) that

$$S(U_h, V_a + V_b, N_a + N_b) \leq S(U_a + U_b, V_a + V_b, N_a + N_b)\,. \tag{3.34}$$

Hence, since *S* is a monotonic increasing function of *U* at constant *V* and *N*, one concludes that $U_h \leq U_a + U_b$, or

$$U(S_a + S_b, V_a + V_b, N_a + N_b) \leq U(S_a, V_a, N_a) + U(S_b, V_b, N_b)\,. \tag{3.35}$$

Thus Ω is stable against internal processes leading to inhomogeneity provided it has no partitioned state of lower energy at constant entropy. This condition is equivalent to Eq. (3.30) but more convenient to use.

To illustrate Eq. (3.35) suppose $V_a = V_b = V,\ N_a = N_b = N$ and consider the stability condition for Ω under a transfer of entropy between Ω_a and Ω_b. Let $S_a = S + \delta S,\ S_b = S - \delta S$; Ω will be stable under this perturbation provided:

$$U(2S, 2V, 2N) \leq U(S + \delta S, V, N) + U(S - \delta S, V, N),$$

or

$$U(S, V, N) \leq \frac{1}{2}\{U(S + \delta S, V, N) + U(S - \delta S, V, N)\}. \tag{3.36}$$

This equation has a simple geometric interpretation. The right-hand side represents *U* at the midpoint of a straight line in the *U*-*S* plane joining the points with coordinates $(U(S + \delta S), S + \delta S)$ and $(U(S - \delta S), S - \delta S)$, as shown in figure 3.1. The left-hand side is the corresponding equilibrium value of *U*. Thus any chord connecting two points on the locus of equilibrium states

in the *U*-*S* plane must lie above the locus. Such functions are said to be convex (meaning convex-down). If the chord lies below the curve, the function is concave. If a concave function is twice differentiable, its second derivative is either negative or zero. For a convex function, its second derivative is either positive or zero. Thus, for the system to be stable *U* must be a convex function of S at constant *V* and *N*. It also follows from Eq. (3.35) that *U* must be a convex function of *V* and *N* and this condition must hold for large as well as small variations, δS, δV and δN.

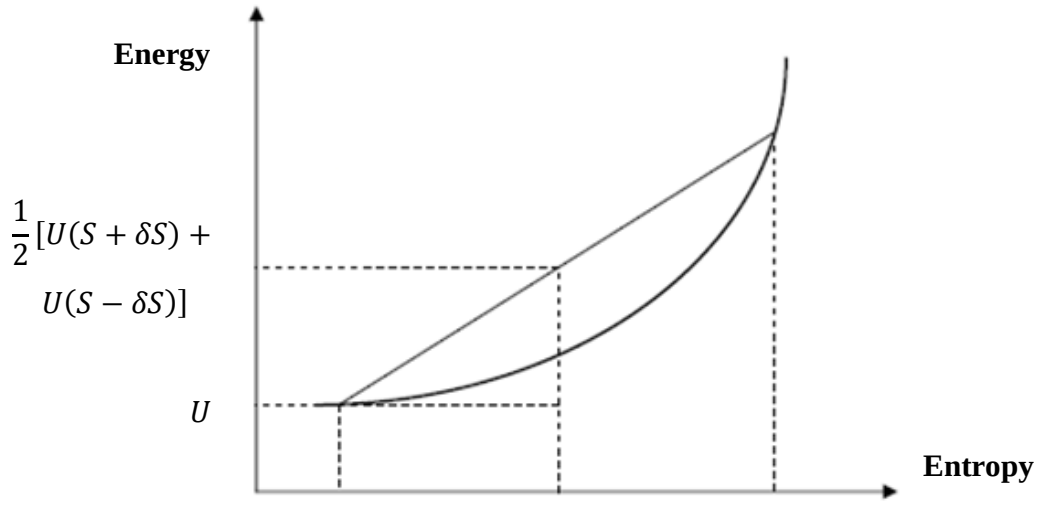

Figure 3.1: Illustrating the curvature condition, Eq. (3.31), that *U* must be a convex-down function of *S* when a single-phase system is stable, from Ref. [44].

Other stability criteria may be obtained from Eq. (3.30) by considering variations in v and g in Eq. (3.25). Assume $S_a = S_b = S$ and consider the stability condition for Ω under transfer of particles and thus volume between Ω_a and Ω_b. Let $v_a = v + \delta v,\ v_b = v - \delta v,\ g_a = g + \delta g,$ $g_b = g - \delta g$; Ω will be stable under this perturbation provided that:

$$u(2v, 2g, 2S) \leq u(v + \delta v, g + \delta g, S) + u(v - \delta v, g - \delta g, S), \tag{3.37}$$

or

$$u(v, g, S) \leq \frac{1}{2}\{u(v + \delta v, g + \delta g, S) + u(v - \delta v, g - \delta g, S)\}. \tag{3.38}$$

Now assume that u is well behaved in the thermodynamic domain of interest so that the terms on the right-hand side of Eq. (3.38) may be expanded as a Taylor series in δv and δg

$$u(v \pm \delta v, g \pm \delta g, S) \simeq u(v,g) \pm \delta v \frac{\partial u}{\partial v} + \delta g \frac{\partial u}{\partial g} + \frac{1}{2}(\delta v)^2 \frac{\partial^2 u}{\partial v^2} + \frac{1}{2}(\delta g)^2 \frac{\partial^2 u}{\partial g^2}$$

$$+ \delta v \delta g \frac{\partial^2 u}{\partial v \delta g}. \tag{3.39}$$

Substituting this expansion into Eq. (3.38) provides the following inequality

$$(\delta v)^2 \frac{\partial^2 u}{\partial v^2} + (\delta g)^2 \frac{\partial^2 u}{\partial g^2} + 2\delta v \delta g \frac{\partial^2 u}{\partial v \delta g} \geq 0. \tag{3.40}$$

By introducing the symmetric 2×2 matrix Π whose elements are second derivatives of u, condition 3.39 can be expressed in matrix form [44, 45]:

$$\Pi = \begin{pmatrix} \frac{\partial^2 u}{\partial v^2} & \frac{\partial^2 u}{\partial v \delta g} \\ \frac{\partial^2 u}{\partial g \delta v} & \frac{\partial^2 u}{\partial g^2} \end{pmatrix} = \begin{pmatrix} u_{vv} & v_{vg} \\ u_{gv} & u_{gg} \end{pmatrix}, \quad v_{vg} = u_{gv}\,. \tag{3.41}$$

Introducing the two component vector, $y = (\delta v, \delta g)$, and its transpose, $y^T \Pi y \geq 0$, which means that the matrix Π must be positive definite. By definition, a symmetric $Z \times Z$ matrix, R_{ij}, is said to be positive if for any vector y with components $y_i, i = 1, \ldots, Z$

$$y^T R y = \sum_{i,j=1}^{Z} y_i \, R_{ij} y_j \geq 0. \tag{3.42}$$

The matrix Π will be positive definite if and only if all its eigenvalues are positive. A necessary and sufficient condition that Π has positive eigenvalues is that a number of minors of the determinant be positive:

$$\begin{vmatrix} \frac{\partial^2 u}{\partial v^2} & \frac{\partial^2 u}{\partial v \delta g} \\ \frac{\partial^2 u}{\partial g \delta v} & \frac{\partial^2 u}{\partial g^2} \end{vmatrix} \geq 0 \ \ and \ \ \left(u_{vv} + u_{gg} \geq 0\right). \tag{3.43}$$

For Eq. (3.43) to be true, $u_{vv} \geq 0$ and $u_{gg} \geq 0$. Using Eq. (3.27) allows one to express the positivity (stability) conditions in terms of the following inequalities

$$-\left(\frac{\partial P}{\partial v}\right)_{\mu} > 0\,, \tag{3.44}$$

and

$$-\left(\frac{\partial \mu}{\partial g}\right)_{v} > 0\,. \tag{3.45}$$

At a fixed μ, the mechanical stability condition of the system is expressed by Eq. (3.44). The positivity of Eq. (3.44) means that baryon density fluctuations are stable, ensuring that any local density fluctuation will not diverge. To ensure that charge fluctuations are stable and obey charge neutrality, Eq. (3.45) has to be positive. When Eq. (3.45) becomes negative, the phase is no longer homogeneous and seperates into phases with different charge density. When beta-equilibrium is reached, i.e. $\mu = \mu_e = \mu_n - \mu_p$, the electron contribution to the pressure P_e only depends on the chemical potential μ, and one can rewrite Eq. (3.44) to include only the baryon contribution to the pressure P_b:

$$-\left(\frac{\partial P_b}{\partial v}\right)_\mu > 0, \tag{3.46}$$

where

$$P_b = \rho^2 \frac{\partial E_b(\rho, x_p)}{\partial \rho}. \tag{3.47}$$

By using the relation $\frac{\partial E_b(\rho,x_p)}{\partial x_p} = -\mu$ together with Eq. (3.47), one can obtain the stability conditions expressed by Eq. (3.45) and Eq. (3.46) only in terms of the baryonic contribution (E_b) to the total energy [39]

$$-\left(\frac{\partial P_b}{\partial v}\right)_\mu = 2\rho^3 \frac{\partial E_b(\rho, x_p)}{\partial \rho} + \rho^4 \frac{\partial^2 E_b(\rho, x_p)}{\partial \rho^2} - \rho^4 \left(\frac{\partial^2 E_b(\rho, x_p)}{\partial \rho \partial x_p}\right)^2 \Big/ \frac{\partial^2 E_b(\rho, x_p)}{\partial x_p^2}. \tag{3.48}$$

$$-\left(\frac{\partial g}{\partial \mu}\right)_v = 1 \Big/ \frac{\partial^2 E_b(\rho, x_p)}{\partial x_p^2} + \frac{\partial \rho_e}{\partial \mu_e} \Big/ \rho \tag{3.49}$$

where $g = x_p - \frac{\rho_e}{\rho}$. The $\rho = \frac{1}{v}$ is the baryon density and the $E_b(\rho, x_p)$ is the energy per baryon. By using the free Fermi gas model, the density of electrons ρ_e is shown to be determined by the electron chemical potential; $\mu_e = \sqrt{\hbar^2 (3\pi^2 \rho_e)^{2/3} + m_e^2}$ and Eq. (3.48) can be written in terms of μ_e. Eq. (3.47) and Eq. (3.48) then become

$$-\left(\frac{\partial P_b}{\partial v}\right)_\mu = \rho^2 \left[2\rho \frac{\partial E_b(\rho, x_p)}{\partial \rho} + \rho^2 \frac{\partial^2 E_b(\rho, x_p)}{\partial \rho^2} - \left(\frac{\partial^2 E_b(\rho, x_p)}{\partial \rho \partial x_p}\right)^2 \Big/ \frac{\partial^2 E_b(\rho, x_p)}{\partial {x_p}^2}\right] > 0, \tag{3.50}$$

$$-\left(\frac{\partial g}{\partial \mu}\right)_v = 1 \Big/ \frac{\partial^2 E_b(\rho, x_p)}{\partial x_p^2} + \frac{\mu_e^2}{\pi^2 \hbar^3 \rho} > 0. \tag{3.51}$$

Eq. (3.50) is always true. The transition density is then determined from Eq. (3.50) at the density where $-\left(\frac{\partial P_b}{\partial v}\right)_\mu = 0$.

$$V_{ther} = 2\rho\frac{\partial E_b(\rho, x_p)}{\partial \rho} + \rho^2\frac{\partial^2 E_b(\rho, x_p)}{\partial \rho^2} - \left(\frac{\partial^2 E_b(\rho, x_p)}{\partial \rho \partial x_p}\right)^2 \Bigg/ \frac{\partial^2 E_b(\rho, x_p)}{\partial x_p^2} > 0. \tag{3.52}$$

3.4 The relationship between the dynamical and thermodynamical methods

Eq. (3.23) and Eq. (3.52) together with the relationship between the density ρ and the proton fraction x_p required by beta-equilibrium and the charge neutrality conditions determine respectively the dynamical and the thermodynamical core-crust transition density in neutron stars. The relationship between these two methods is still unclear although they have been widely used in the literature. Here it will be shown that thermodynamical method corresponds to the long-wavelength limit of the dynamical one when the Coulomb interaction is neglected.

The stability conditions are usually expressed using the ρ and x_p within the dynamical method while the $\rho_n = (1 - x_p)\rho$ and $\rho_p = x_p\rho$ is used within the thermodynamical one. By neglecting the beta-equilibrium and charge neutrality conditions and using the following thermodynamical relations, the relationship between the two methods become clearer [40]

$$\frac{\partial E_b}{\partial x_p} = -\mu = \mu_p - \mu_n\,, \tag{3.53}$$

$$\frac{\partial P_b}{\partial \rho} = (1 - x_p)\rho\frac{\partial \mu_n}{\partial \rho} + x_p\rho\frac{\partial \mu_p}{\partial \rho}\,, \tag{3.54}$$

$$\frac{\partial P_b}{\partial x_p} = (1 - x_p)\rho\frac{\partial \mu_n}{\partial x_p} + x_p\rho\frac{\partial \mu_p}{\partial x_p}\,, \tag{3.55}$$

where the pressure of baryons is $P_b = \mu_n \rho_n + \mu_p \rho_p - E_b \rho$. The derivatives of the energy of baryons can now be expressed as

$$\frac{\partial E_b}{\partial \rho} = \frac{P_b}{\rho^2}, \tag{3.56}$$

$$\begin{aligned}\frac{\partial^2 E_b}{\partial \rho^2} &= \frac{\partial}{\partial \rho}\left(\frac{P_b}{\rho^2}\right) \\ &= -\frac{2P_b}{\rho^3} + \frac{1}{\rho^2}\left[(1-x_p)\rho\frac{\partial \mu_n}{\partial \rho} + x_p \rho \frac{\partial \mu_p}{\partial \rho}\right] \\ &= -\frac{2P_b}{\rho^3} + \frac{1}{\rho^2}\left[(1-x_p)^2 \rho\frac{\partial \mu_n}{\partial \rho_n} + x_p(1-x_p)\frac{\partial \mu_n}{\partial \rho_p}\right] \\ &\quad + \frac{1}{\rho^2}\left[x_p(1-x_p)\rho\frac{\partial \mu_p}{\partial \rho_n} + x_p^2 \rho \frac{\partial \mu_p}{\partial \rho_p}\right],\end{aligned} \tag{3.57}$$

$$\begin{aligned}\frac{\partial^2 E_b}{\partial x_p^2} &= -\frac{\partial \mu}{\partial x_p} = \frac{\partial \mu_p}{\partial x_p} - \frac{\partial \mu_n}{\partial x_p} \\ &= \rho\left(\frac{\partial \mu_p}{\partial \rho_p} - \frac{\partial \mu_p}{\partial \rho_n} - \frac{\partial \mu_n}{\partial \rho_p} + \frac{\partial \mu_n}{\partial \rho_n}\right),\end{aligned} \tag{3.58}$$

$$\begin{aligned}\frac{\partial^2 E_b}{\partial \rho \partial x_p} &= -\frac{\partial \mu}{\partial \rho} = \frac{\partial \mu_p}{\partial \rho} - \frac{\partial \mu_n}{\partial \rho} \\ &= (1-x_p)\frac{\partial \mu_p}{\partial \rho_n} + x_p \frac{\partial \mu_p}{\partial \rho_p} - (1-x_p)\frac{\partial \mu_n}{\partial \rho_n} - x_p \frac{\partial \mu_n}{\partial \rho_p}.\end{aligned} \tag{3.59}$$

By neglecting the Coulomb interaction the following relation holds for nuclear matter

$$\frac{\partial \mu_n}{\partial \rho_p} = \frac{\partial \mu_p}{\partial \rho_n}. \tag{3.60}$$

By using Eq. (3.55), (3.56), (3.57) and (3.58) in Eq. (3.59), the following equality is obtained

$$\frac{2}{\rho}\frac{\partial E_b}{\partial \rho}\frac{\partial^2 E_b}{\partial x_p^2} + \frac{\partial^2 E_b}{\partial \rho^2}\frac{\partial^2 E_b}{\partial x_p^2} - \left(\frac{\partial^2 E_b}{\partial \rho \partial x_p}\right)^2 = \frac{\partial \mu_n}{\partial \rho_n}\frac{\partial \mu_p}{\partial \rho_p} - \left(\frac{\partial \mu_n}{\partial \rho_p}\right)^2. \tag{3.61}$$

From Eq. (3.60) it can be seen that for $\frac{\partial^2 E_b}{\partial x_p^2}$ to be positive, the first term in Eq. (3.61) must be positive meaning that the condition expressed by Eq. (3.50) is equivalent to requiring a positive bulk term V_0 in Eq. (3.19). By taking the limit of the dynamical stability condition Eq. (3.17) as $k \to 0$ and neglecting the Coulomb interaction, the thermodynamical stability condition, the right hand side of Eq. (3.61) is reproduced.

3.5 Summary

In this chapter two methods for calculating the crust-core transition density were studied. The core region of the neutron star is considered to be a homogeneous liquid while the crustal region is a non-uniform solid structure. The methods work by studying how the system's free-energy changes from the core to the crust when small-amplitude density fluctuations are introduced, thus moving gradually across the transition density. It was found that the homogeneous liquid core becomes unstable if the introduced density fluctuation reduces the free-energy of the system. It was also found that the thermodynamical stability condition is the limit of the dynamical one as $k \to 0$ when the Coulomb interaction is neglected. The emphasis of this project is on the Skyrme interaction used within the dynamical method. The next chapter focuses mainly on this, where interpretation of graphs and results are discussed.

CHAPTER 4
Results and discussion

In chapter 3 the Skyrme interaction was used within the dynamical method to derive a condition for finding the crust-core transition density. The instability boundary can be calculated by determining the density at which Eq. (3.23) becomes zero. This was done numerically in a FORTRAN90 code using the EOS of symmetric nuclear matter for fifteen parameter sets (given in Table. 2.1) of the Skyrme interaction. Properties of saturated symmetric nuclear matter were calculated and the transition density was determined for the parameter sets, each showing unique behaviour. These properties include the saturation density (ρ_0), binding energy (E_0), symmetry energy ($E_{sym}(\rho_0)$) and the slope (L) and incompressibility (curvature, K) parameters of the symmetry energy at the saturation density. Differences in the behaviour of the parameter sets are discussed in this chapter and results are compared with published values and also observational properties of neutron stars.

Table 4.1 shows the properties of neutron stars using the Skyrme interaction, including the transition density. These results are in excellent agreement with published values given in Ref. [40]. The saturation density ranges from $0.145\ fm^{-3}$ to $0.16\ fm^{-3}$ and the symmetry energy ranges from $27.8\ MeV$ to $33.2\ MeV$ which are consistent with their empirical values inferred from nuclear laboratory data, thus validating the use of the Skyrme interactions for describing nuclear matter. Figure 4.1 shows the binding energy as a function of baryon density, the Skyrme interactions all have similar behaviour below saturation density, after which they start to deviate. There is a direct relation between the energy density (thus energy per nucleon), the symmetry energy and curvature. If the energy per nucleon increases rapidly with density, the EOS is said to be stiff, if the increase is more gradual it is known as soft. In Figure 4.1 it can be seen that there is one parameter set showing strong deviation from the rest. This parameter set is SIII, it has a stiff EOS which is indicated by the rapid increase of the energy per nucleon as a function of density. Notice also the lowest E_{sym} curve in figure 4.2 corresponding to SIII. On the other hand SKI3 has the lowest, softest E_0 curve and the highest, stiffest E_{sym} curve. E_{sym} is proportional to the second derivative of E_0 with respect to the density. In turn the curvature is proportional to the second derivative of E_{sym}. Thus, the stiffer the binding energy of a parameter set, the softer the

symmetry energy, the smaller the curvature and the greater the transition density as seen in Table 4.1. The parameter set with the smallest curvature has a bigger transition density and the one with the biggest curvature has the smallest transition density. Thus the transition density also depends on the symmetry energy. The transition density ranges from $0.06\ fm^{-3}$ to $0.12\ fm^{-3}$ within the dynamical method by using Skyrme interactions, as seen from Figures 4.3 and 4.4.

Skyrme	$\rho_0(fm^{-3})$	$E_0(\rho_0)(MeV)$	$E_{sym}(\rho_0)(MeV)$	L (MeV)	K (MeV)	$\rho_t(fm^{-3})$
BSK1	0.157	-15.8	27.8	7.2	-281.8	0.12
SKP	0.163	-16.0	30.0	19.6	-266.8	0.10
SKM*	0.160	-15.8	30.0	45.8	-155.9	0.075
SLy230a	0.160	-16.0	32.0	44.3	-98.2	0.08
SIII	0.145	-15.9	28.2	9.9	-393.7	0.11
SLy230b	0.160	-16.0	32.0	46.0	-119.7	0.08
Sly6	0.161	-16.5	32.2	46.7	-117.0	0.08
SKM	0.160	-15.8	30.7	49.3	-148.8	0.078
SGII	0.158	-15.6	26.8	37.6	-145.9	0.078
SKI4	0.160	-15.9	29.5	60.4	-40.6	0.07
SKI3	0.158	-16.0	34.8	100.5	73.0	0.06
SKX	0.155	-16.1	31.1	33.2	-252.1	0.088
SKXce	0.155	-15.9	30.1	33.5	-238.4	0.09
SKXm	0.159	-16.0	31.2	32.1	-242.8	0.092
SkSC4	0.161	-15.9	28.8	-2.2	-329.5	_
Observed	0.153	-16.3	32.5	52.7	_	_

Table 4.1: Symmetric nuclear matter properties for different parameter sets of the Skyrme interaction compared to the observational properties.

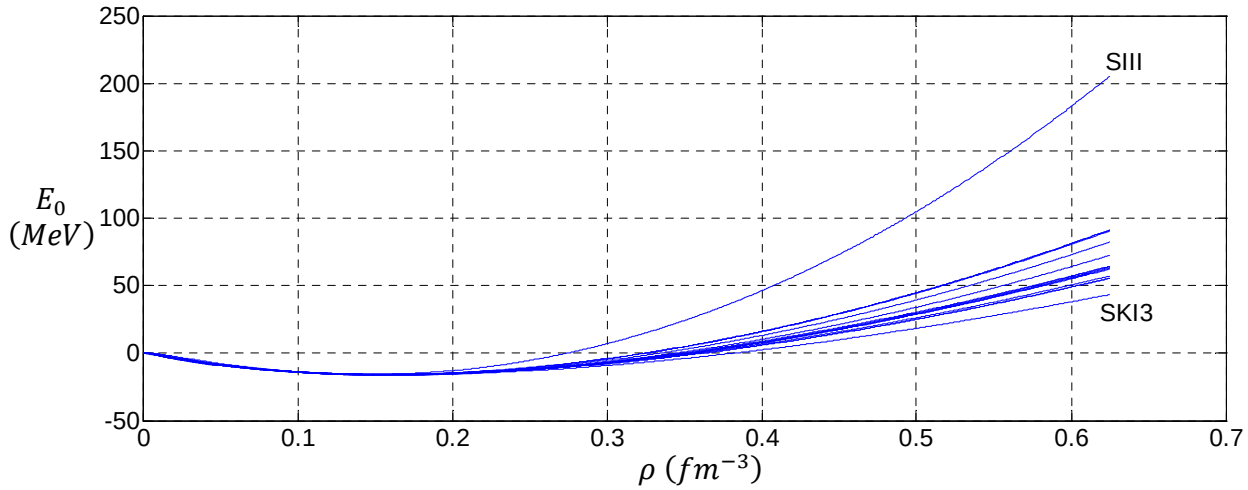

Figure 4.1: Energy per nucleon for fifteen parameter sets of the Skyrme interaction for symmetric nuclear matter.

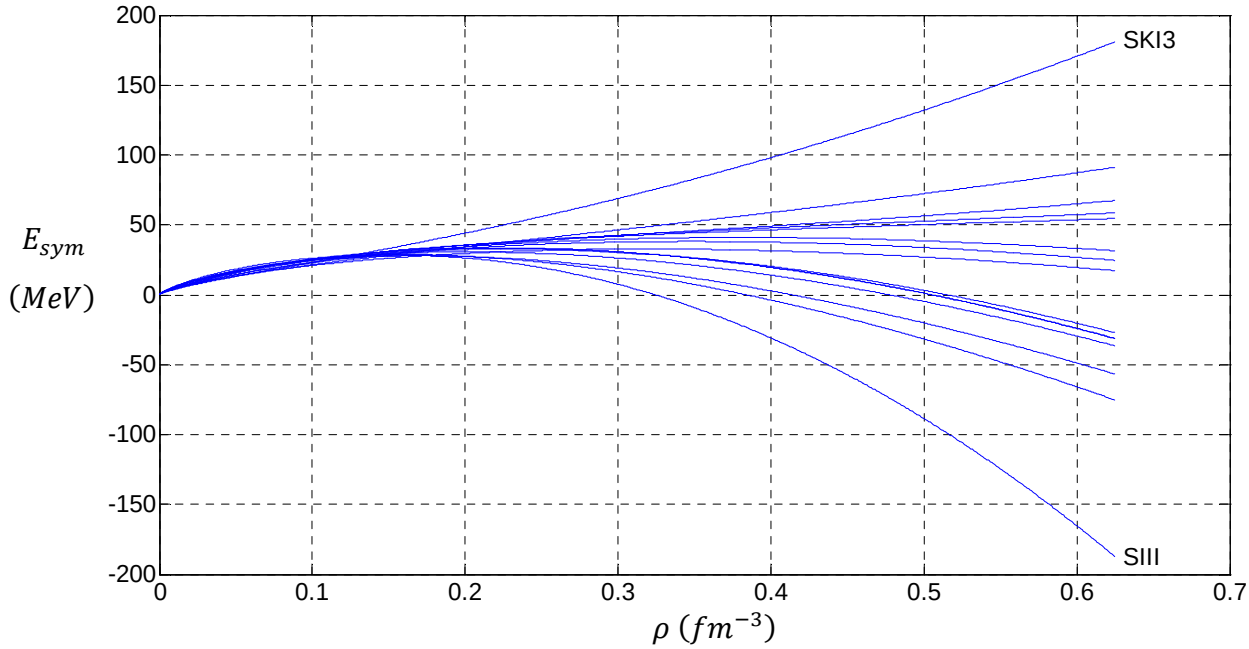

Figure 4.2: The density dependence of symmetry energy for different Skyrme interactions.

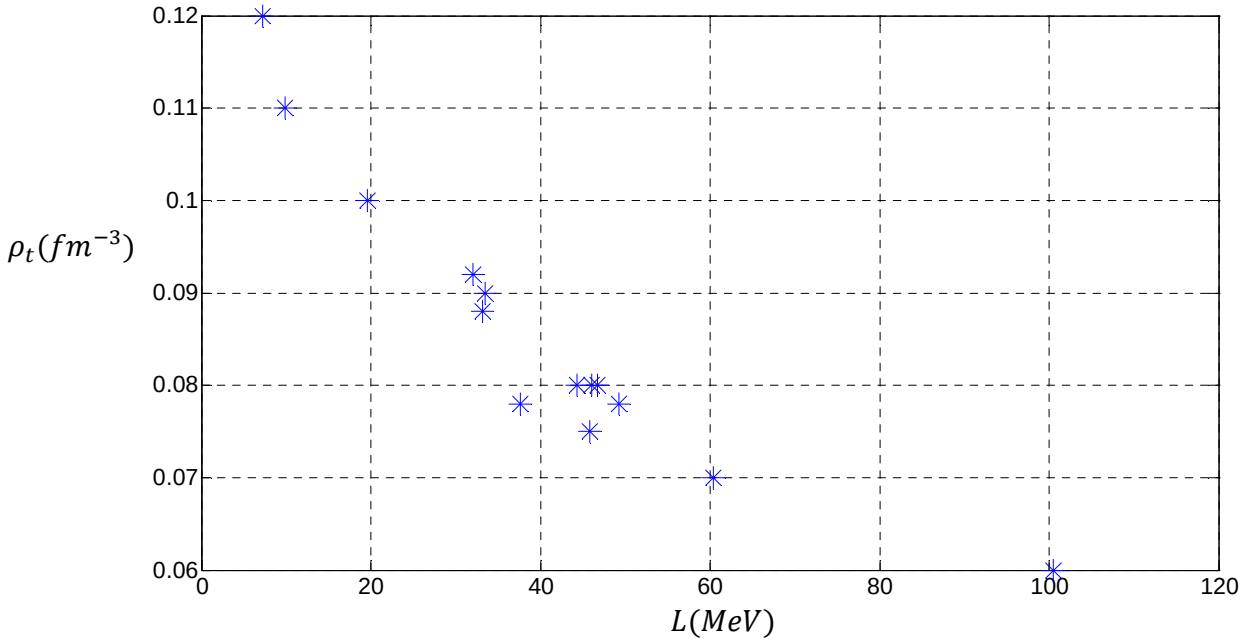

Figure 4.3: The transition density as a function of L by using the dynamical method with Skyrme interactions.

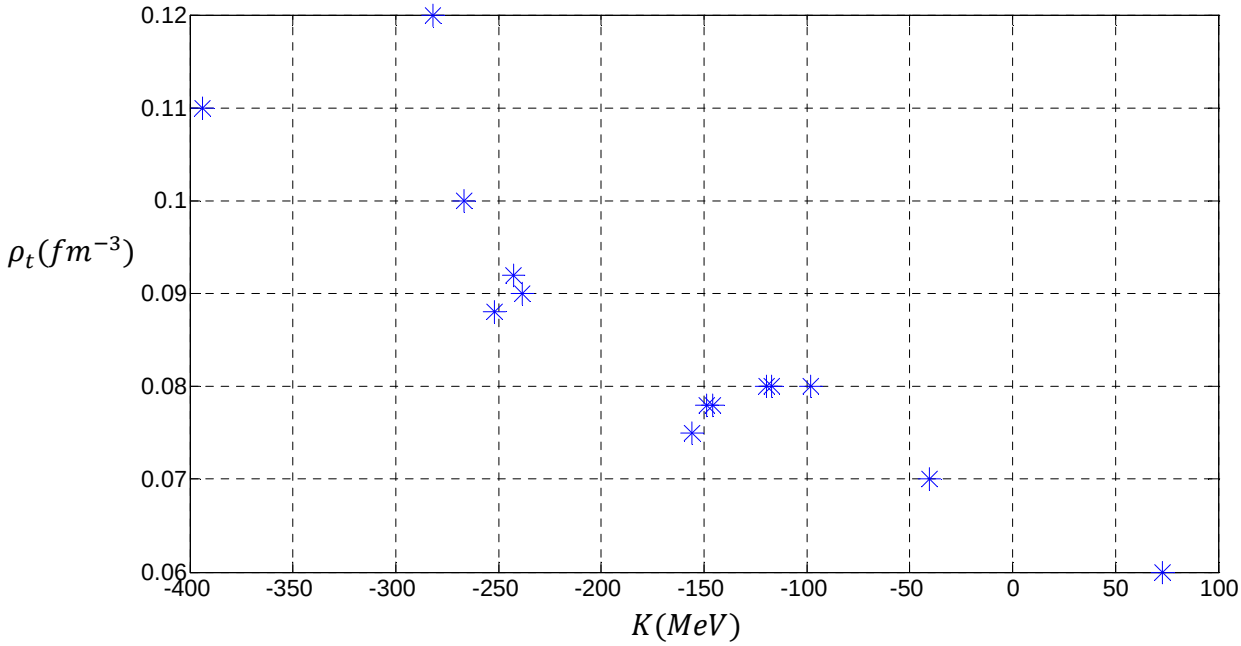

Figure 4.4: The transition density as a function of *K* by using the dynamical method with Skyrme interactions.

For Skyrme parameter sets where L < 7 MeV, the transition density does not exist, meaning the *npe* matter is always unstable. The transition density is very sensitive to the density dependence of the symmetry energy, which can be well characterized by the slope *L* and the incompressibilty coefficient *K*. The variation in the transition density with *K* is very similar to that with *L*, as seen from figures 4.3 and 4.4, indicating a correlation between *K* and *L*. It should be noticed that the selected Skyrme parameter sets present a behaviour of values of *L* lower than 60 MeV, while recent constraints extracted from different experimental analysis indicate that *L* should be larger than about 60 MeV [46]. The density dependence of the symmetry energy is less constrained by experimental data [47], and shows very different behaviour with the different parameterizations shown in figure 4.2. The differences in behaviour stem from the different parameter values which are chosen to fit the binding energies and charge radii of a large number of nuclei in the periodic table. Figure 4.5 shows the effect of the parameter x on the symmetry energy in the momentum dependent interaction, with the curves intersecting at the saturation density (ρ_0= 0.16 fm^{-3}).

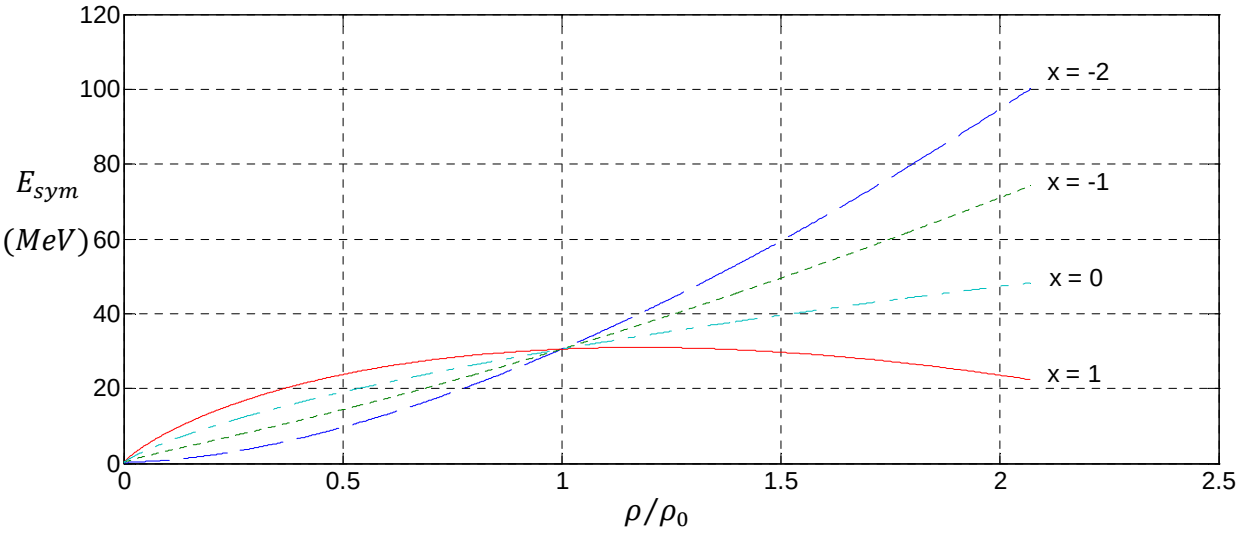

Figure 4.5: The density dependence of the nuclear symmetry energy for different values of the parameter *x* in the MDI interaction.

In summary, the fifteen parameter sets of the Skyrme interaction reproduce the observational properties of neutron stars, such as binding energy, saturation density, incompressibility

coefficient and symmetry energy, very well below saturation density. The behaviour of the EOS of each parameter set is unique, although the saturation properties they produce are in close agreement. At densities above saturation their behaviour starts to deviate drastically. This shows the importance of finding a model and thus also EOS which is capable of describing nuclear matter not only at sub-saturation densities but also in the supra-density realm of which current knowledge is minimal. It was shown that the transition density depends on the symmetry energy, which is characterized by the slope and curvature. The transition density was only an approximation and is essential for understanding pulsar glitches as described in chapter one, thus it is critical to find a more accurate EOS and model for describing nuclear interactions in stars.

CHAPTER 5

Summary and Conclusions

In summary, two methods for finding the crust-core transition density were studied. EOS's were constructed using fifteen of the most popular Skyrme interaction parameter sets used in the literature and a modified Gogny interaction (MDI) was briefly discussed, with the idea to use these interactions within the dynamical and thermodynamical methods to determine the transition density between the crust and core of a neutron star in its ground state. It was shown that the dynamical and thermodynamical methods are related; the thermodynamical stability condition corresponds to the long-wavelength limit of the dynamical method when the Coulomb interaction is neglected. Some observable properties of neutron stars were reproduced using the fifteen different Skyrme interaction parameter sets, validating the use of the Skyrme interactions. The two parameter sets which give the closest agreement with the observable properties are SKX and SKXce. The transition density was found to be very sensitive to the density dependence of the nuclear symmetry energy. The different Skyrme interaction parameter sets gave different values for the transition density, ranging from $0.06\ fm^{-3}$ to $0.12\ fm^{-3}$ within the dynamical method, showing good agreement with those published in Refs. [8] and [40]. The fifteen Skyrme parameter sets show similar behaviour below saturation, but start to deviate drastically at higher densities. The range of the transition density found in this work indicate that there is still much uncertainty associated with it. Of course different neutron stars will have different transition densities, but the different models used to describe a particular neutron star should at least show good agreement with each other. Hopefully advances in radioactive nuclear beam facilities will provide the possibility to better understand the density dependence of the nuclear symmetry energy in heavy ion collisions induced by these nuclei. The thickness of the neutron skin in heavy nuclei such as lead (*Pb*) can be linked to the slope of nuclear matter symmetry energy at saturation density and is believed to contain information on the density dependence of the nuclear symmetry energy [46]. This has not been possible due to the large uncertainties in measured neutron skin thickness of heavy nuclei. Values of the slope can also be extracted by determining the density dependence of the nuclear symmetry energy from the isospin diffusion data in heavy-ion collisions. Limits on the allowed parameter sets for the Skyrme interaction can then be set.

This project opens the door for a number of future endeavours. The modified Gogny interaction can be studied within the dynamical and thermodynamical methods for determining the transition density. The Skyrme interaction can also be used within the thermodynamical method not only for symmetric nuclear matter but also asymmetric nuclear matter. Other models such as the Relativistic Mean-field approximation applied to Quantum Hadrodynamics (QHD) could also be studied and compared with the Skyrme and modified Gogny interactions in the pursuit of finding an accurate model for describing nuclear structure and constraining the EOS. There are proposals that the crust-core transition region may contain plate- and rod-like structures [9, 10] and that the nuclear shape changes from spherical to non-spherical, making the describtion of nuclear matter more complicated if these shapes are included, because laboratory data on nuclei reflect only the bulk and surface properties of nearly symmetric nuclear matter. The transition density is also important for understanding pulsar glitches which are associated with a sudden change in its moment of inertia and is required to determine the moment of inertia of the different parts of the neutron star interior.

Currently the knowledge base in South Africa pertaining to models that describe the interior of pulsars and neutron stars, from the nuclear perspective, is very limited. The success of nuclear models depends on their ability to reproduce known observables, this is why the Square Kilometre Array is so important; it could be used to observe neutron star properties and collect neutron star data that can be used to constrain these models. In particular, existing data of glitching in the Vela pulsar from Hartebeeshoek Radio Astronomy Observatory (HartRAO) can be used. The Square Kilometre Array will provide exposure to current neutron star research by providing opportunities for hands-on experience, not only theoretical. It is important to combine theoretical models with experimental data in order to improve the theoretical models.

BIBLIOGRAPHY

[1] Andrew Lyne and Francis Graham-Smith, *Pulsar Astronomy*, 3rd edition, Cambridge University Press, (2006).

[2] D.G. Yakovlev, Phys. Usp. **44**, 823 (1999).

[3] N.K. Glendenning, *Compact stars*, 2nd edition, Springer, (2000).

[4] S.L. Shapiro and S.A. Teukolsky, *Black Holes, White Dwarfs, and Neutron stars*, John Wiley & Sons, (1983).

[5] H.-Th. Janka, K. Langanke, A. Mareka, G. Martínez-Pinedo and B. Müller, Phys. Rep. **442**, 38 (2007).

[6] D.G. Yakovlev, A.D. Kaminker, O.Y. Gnedin and P. Haensel, Phys. Rep. **354**, 1 (2001).

[7] S. B. Rüster, M. Hempel, and J. Schaffner-Bielich, arXiv:0509325v2 [astro-ph].

[8] C.J. Pethick, D.G. Ravenhall and C.R Lorenz, Nuc. Phys. **A584**, 675 (1995).

[9] K. Oyamatsu, Nuc. Phys. **A561**, 431 (1993).

[10] K. Oyamatsu and K. Iida, Phys. Rev. C **75**, 015801 (2007).

[11] F. Douchin and P. Haensel, Phys. Lett. **B 485**, 107 (2000) .

[12] N. Chamel, arXiv:0512034v1 [nucl-th].

[13] F. Douchin, P. Haensel and J. Meyer, Nuc. Phys. **A665**, 419 (2000).

[14] http://www.astroscu.unam.mx/neutrones/NS-picture/NStar/NStar-I.gif.

[15] D.H. Youngblood, H.L. Clark, and Y.W. Lui, Phys. Rev. Lett. **82**, 691 (1999).

[16] S. Shlomo, V.M Kolomietz, and G. Col`o, Eur. Phys. J. A **30**, 23 (2006).

[17] P. Danielewicz, R. Lacey, and W.G. Lynch, Science **298**, 1592 (2002).

[18] J. Aichelin and C.M. Ko, Phys. Rev. Lett. **55**, 2661 (1985).

[19] C. Fuchs, Prog. Part. Nucl. Phys. **56**, 1 (2006).

[20] W.D. Myers and W.J Swiatecki, Nucl. Phys. **A81**, 1 (1966).

[21] V. Pomorski and J. Dudek, Phys. Rev. C **67**, 044316 (2003).

[22] Y. Yano, Nucl. Instr. Meth. **B261**, 1009 (2007).

[23] http://www.gsi.de/fair/index e.html

[24] http://ganinfo.in2p3.fr/research/developments/spiral2

[25] http://dnp.aps.org

[26] J. Carriere, C. J. Horowitz and J. Piekarewicz, arXiv:0211015v1 [nucl-th].

[27] B. Link, R.I. Epstein and J.M. Lattimer, Phys. Rev. Lett. **83**, 17 (1999).

[28] E. Chabanat, E. Bonche, E. Haensel, J. Meyer and R. Schaeffer, Nucl. Phys. **A627**, 710 (1997).

[29] J.R. Stone, P.-G. Reinhard, Prog. Part. Nucl. Phys **58**, 587 (2007).

[30] B.D. Serot and J.D. Walecka, Adv. Nuc. Phys. 16, 1 (1986).

[31] C. B. Das, S. Das Gupta, C. Gale and Bao-An Li, Phys. Rev. **C67**, (2003).

[32] http://physicsworld.com/cws/article/print/1497

[33] T. H. R. Skyrme, Phil. Mag. **1**, 1043 (1956).

[34] T. H. R. Skyrme, Nucl. Phys. **9**, 615 (1959).

[35] D. Vautherin and D. M. Brink, Phys. Lett. **32B**, 149 (1970).

[36] D. Vautherin and D. M. Brink, Phys. Rev. **C5**, 626 (1972).

[37] M. Brack, C. Guet and Hakansson, Phys. Rep. **123**, 275 (1985).

[38] J.Friedrich and P.-G. Reinhard, Phys. Rev. **C33**, 335 (1986).

[39] B. Brown, Phys. Rev. **C58**, 220 (1998).

[40] J. Xu, L.W. Chen, B.A. Li and H.R. Ma, arXiv:0901.2309v1 [astro-ph].

[41] C. Ducoin, J. Margueron and Ph. Chomaz, Nucl. Phys. **A809**, 30 (2008).

[42] H. Anton and C. Rorres, *Elementary linear algebra*, 8th edition, John Wiley & Sons, (2000).

[43] G. Baym, H. Bethe and C.J. Pethick, Nucl. Phys. **A175**, 225 (1971).

[44] Gerald Carrington, *Basic Thermodynamics*, Oxford University Press, (1994).

[45] Dieter. H.E. Gross, *Microcanonical Thermodynamics*, World Scientific Publishing, (2001).

[46] L.W. Chen, C. Ko and B.A. Li, Phys. Rev. **C72,** 064309 (2005).

[47] Baran, Phys. Rep. **410,** 335 (2005).

APPENDIX A

Code Documentation

To calculate the properties of neutron stars and find the crust-core transition density a program was written in the FORTRAN90 programming language. Plots were made in the MATLAB programming language by exporting the data generated by the program. In this section a description of the program is given.

A.1 The main program

The main program consists of a program called SKYRME and subroutines for each SKYRME parameter set. The SKYRME program contains the values of Fermi momenta. It asks the user to enter a number corresponding to which SKYRME parameter set the user would like to use to calculate the neutron star properties for symmetric nuclear matter using the dynamical method. The SKYRME program then calls the corresponding subroutine, sending the Fermi momenta to the subroutine and displays the results on screen.

There are fifteen SKYRME parameters sets, each corresponding to a different number:

SIII - 1
SKP - 2
SLy230a - 3
SLy230b - 4
SKM* - 5
SKM - 6
SKXm - 7
SKI3 - 8
SKI4 - 9
SLy6 - 10
BSK1 - 11
SGII - 12
SKX - 13

SKXce - 14
SkSC4 - 15

Each subroutine operates in the same way. It calculates the proton and neutron densities from the Fermi momenta and calculates the energy per nucleon and symmetry energy at each baryon density and saves the values in a file for plotting in MATLAB. The subroutine searches for the saturation density, where the energy per nucleon is a minimum, and calculates the slope and incompressibility parameters of the symmetry energy, L and K, at the saturation density. The chemical potentials are also calculated at each Fermi momentum, and used in Eq. 3.23 to find where this equation becomes zero and thus finding the transition density.